



Contents lists available at ScienceDirect

Journal of the Mechanics and Physics of Solids

journal homepage: www.elsevier.com/locate/jmps

A micromechanically motivated diffusion-based transient network model and its incorporation into finite rubber viscoelasticity

Christian Linder*, Mykola Tkachuk, Christian Miehe

Institute of Applied Mechanics (CE) Chair I, University of Stuttgart, 70550 Stuttgart, Pfaffenwaldring 7, Germany

ARTICLE INFO

Article history:

Received 30 August 2010

Accepted 16 May 2011

Available online 24 May 2011

Keywords:

Rubber viscoelasticity

Transient network theories

Micromechanics

Brownian motion

Non-equilibrium thermodynamics

ABSTRACT

This paper presents the development of a physical-based constitutive model for the representation of viscous effects in rubber-like materials. The proposed model originates from micromechanically motivated diffusion processes of the highly mobile polymer chains described within the formalism of Brownian motion. Following the basic assumption of accounting for the elastic and the viscous effects in rubber viscoelasticity by their representation through a separate elastic ground network and several viscous subnetworks, respectively, the kinetic theory of rubber elasticity is followed and extended to represent also the viscous contribution in this work. It is assumed that the stretch probability of certain chain segments within an individual viscous subnetwork evolves based on the movement of the chain endpoints described by the Smoluchowski equation extended in this work from non-interacting point particles in a viscous surrounding to flexible polymer chains. An equivalent tensorial representation for this evolution is chosen which allows for the closed form solution of the macroscopic free energy and the macroscopic viscous overstress based on a homogenization over the probability space of the introduced micro-objects. The resulting model of the viscous subnetwork is subsequently combined with the non-affine micro-sphere model and applied in homogeneous and non-homogeneous tests. Finally, the model capacity is outlined based on a comparison with in the literature available experimental data sets.

© 2011 Elsevier Ltd. All rights reserved.

1. Introduction

Polymers are characterized by remarkable properties making them qualified for applications in all areas of engineering. They can appear in liquid or amorphous solid form, behave ductile in the case of glassy polymers or rubber-like for elastomers. The latter, to be considered in this work, can in particular be characterized by the large deformations they can sustain as well as the rate and history dependence of the resulting stresses in the material. This response is attributed to their peculiar microstructure including a network of highly mobile and flexible polymer chains formed by their three-dimensional cross-linking. From a constitutive modeling point of view the challenge lies in the development of physical-based models to depict this behavior. In that regard one distinguishes *static network theories* for the modeling of elastic effects and *transient network theories* for the modeling of time-dependent effects in rubber-like materials. A brief review of those is provided in Sections 1.1 and 1.2, respectively, before in Section 1.3 the scope of the current work is discussed which lies within the development of a new transient network theory for rubber-like materials. Its incorporation into finite

* Corresponding author. Tel.: +49 711 685 66382; fax: +49 711 685 66347.

E-mail address: linder@mechbau.uni-stuttgart.de (C. Linder).

viscoelastic constitutive models, as well as the resulting implementation and application to realistic experiments and its qualitative comparison with existing experimental data sets are the main contributions of this work.

1.1. Static network theories

Early experimental results in Treloar (1944) indicate the characteristic S-shaped load versus stretch curve for the elastic nature of rubber materials in uniaxial tensile tests in the form of an initially decreasing stiffness of the material and a rapid increase thereafter. The reported deformation range, up to an eightfold extension of the material with an almost full recovery of its initial shape upon unloading, outlines one of their main mechanical characteristics and reason for their applicability in various areas of engineering and material science. Further experimental results are given in Rivlin and Saunders (1951), James et al. (1975), and James and Green (1975), among others. The latter introduced a graphical presentation of the results which allowed for a more convenient fit of the material data of constitutive models in terms of their strain energy function. Inspired by the form of such a function for an isotropic, incompressible, hyperelastic material various strain-invariant based phenomenological expressions are proposed to capture the characteristic response of rubber (Mooney, 1940; Rivlin, 1948; Ogden, 1972; Yeoh, 1993). These empirical theories lack a direct physical justification of the parameters appearing in the proposed expressions of the strain energy function.

On the contrary, the kinetic theory of elasticity (Meyer et al., 1932) accounts for the underlying physics by assuming that the material consists of a large number of polymer chains which do form a static network by being permanently cross-linked at junction points. A chain segment, considered as part of a polymer molecule approximated as an idealized chain of freely rotating links, between two such junction points possesses a large number of possible conformations in terms of translational and rotational degrees of freedom which are driven by the influence of the thermal motion of the chain endpoints. Since the angles between adjacent bonds are considered to be random with equally distributed probability, the bond orientations do not correlate resulting in a Gaussian distribution of the end-to-end vector of an unrestrained chain segment. This probability can then be linked through the Boltzmann relation to the entropy and the free energy of a single chain (Kuhn, 1934, 1936; Guth and Mark, 1934). This, as *Gaussian statistics* denoted background for the single entropic chain segments, is used for the derivation of the *Gaussian network models* (Wall, 1943; Flory and Rehner Jr., 1943; James and Guth, 1943; Troloar, 1943a,b; Flory, 1944) consisting of a highly cross-linked network of such Gaussian chains providing a link of the micromechanical polymer model to macroscopic scales. The agreement of those models with the experimental results are acceptable up to stretch regions where the individual chain segments are far from being fully extended.

Such limitation is overcome in the *non-Gaussian statistics* of Kuhn and Gr \ddot{u} n (1942) and later by Flory (1953) based on their account of the finiteness of the chain extensibility where the modified probability density function of a chain with a certain length and its resulting entropy is expressed in closed form in terms of the inverse Langevin function. An account for such a finite extensibility of the individual chain segments in network models results in so called *non-Gaussian network models*. Examples within that frameworks are the *three-chain model* considered in James and Guth (1943) and Wang and Guth (1952), the *four-chain model* by Treloar (1946) as an extension of the model in Flory and Rehner Jr. (1943), or the more recently developed *eight-chain model* by Arruda and Boyce (1993a) which successfully is able to represent the response of these materials in uniaxial extension and compression, biaxial extension, plane strain compression, and pure shear problems. A *full network theory* is proposed in Treloar (1954) and Treloar and Riding (1979) for uniaxial extension and biaxial tensile deformation, respectively, and extended in Wu and van der Giessen (1993) to fully three-dimensional deformation processes. It is noted that, whereas the three-chain model and the full network theory result in *affine* network formulations, meaning that they preserve the affinity of the network deformation with regard to the macroscopically applied deformation, the remaining *non-affine* network models do come along without such restriction. Chains oriented in the direction of loading display a higher resistance to the stretch when approaching their limiting value compared to other chains in the network. Hence, the internal structure of the polymer becomes heterogeneous which leads to a deviation of chain stretches when compared to those resulting from the macrostrain. Only the non-affine models allow for such adjustment of the polymer microstructure.

Even though the underlying mechanisms of the individual chain segments in these theories account for their finite extensibility, the possible chain conformations in between two junction points is not influenced by the surrounding polymer chain segments. This is on the contrary done within *constrained junction theories* (Ronca and Allegra, 1975; Flory et al., 1976; Flory, 1977; Erman and Flory, 1978; Flory and Erman, 1982) and within *constrained segment theories* (Deam and Edwards, 1976; Heinrich and Straube, 1983, 1984; Edwards and Vilgis, 1988; Heinrich and Kaliske, 1997; Kaliske and Heinrich, 1999). In Miehe et al. (2004) a micromechanically motivated network model, including a micro-tube constraint based on Edwards (1967) to account for the surrounding polymer chains, together with a non-affine micro-to-macro transition based on a homogenization procedure defined on a micro-sphere of space orientations is developed. The resulting framework, called the *non-affine micro-sphere model*, yields an excellent performance in homogeneous and non-homogeneous tests. Further references on the elastic behavior of rubber-like materials can be found in Treloar (1975) and the review articles by Boyce and Arruda (2000) or Marckmann and Verron (2006).

1.2. Transient network theories

Besides the elastic ground response of rubber-like materials, captured by the above outlined static network theories, their behavior is characterized by a finite viscoelastic overstress which governs rate-dependent effects such as relaxation

and creep phenomena as well as frequency dependent hysteresis curves in cyclic loading processes. Experimental observations of such effects are reported in Cotten and Boonstra (1965), Ferry (1980), Sullivan (1986), Lion (1996), Miehe and Keck (2000), or Miehe and Göktepe (2005), among others.

When it comes to the numerical modeling of such phenomena, one again may distinguish purely phenomenological models with a strong focus on the numerical implementation developed within the mechanics and engineering community and approaches originating from physical chemistry and material science where the focus lies on molecular models of these phenomena and their experimental justification by microscopic studies. Within the phenomenological approaches, one can find models based on stress-type variables in the form of convolution integrals in the works of Holzapfel and Simo (1996), Lion (1996), or Kaliske and Rothert (1997). Alternatively, the multiplicative split of the deformation gradient, originally suggested by Lee (1969) in the context of elastoplasticity and by Sidoroff (1974) in non-linear viscoelasticity, into elastic and inelastic parts is used in Lubliner (1985), Simo (1987), Boyce et al. (1988), Reese and Govindjee (1998), Govindjee and Reese (1997), or Bergström and Boyce (1998). The description of the time-dependent viscous effects based on the evolution of viscous metric tensors is chosen in Miehe and Keck (2000). An extension of the above mentioned micro-sphere model of rubber elasticity to account for viscous effects is achieved in Miehe and Göktepe (2005) and Göktepe and Miehe (2008).

An alternative to these continuum approaches are the molecular-based theories. These have been developed recently to describe the viscous behavior of molten polymers and amorphous rubber-like materials. The *bead-spring model* (Bird et al., 1977), the *reptation-type tube models* (De Gennes, 1971; Doi and Edwards, 1986), and the *transient network models* (Green and Tobolsky, 1946; Tanaka and Edwards, 1992) are mentioned as examples in this area. Recently, an increasing activity in combining these two approaches can be observed, resulting in so called micromechanically motivated approaches (Boyce et al., 1989; Arruda and Boyce, 1993b; Bergström and Boyce, 1998).

1.3. Scope of this work

In this context, the current work is concerned with the development of a physically interpretable and fully micromechanically motivated transient network model for the description of the polymer chain movement to describe the viscous effects in rubber-like materials. For polymers, consisting of long-chain molecules as proposed in Staudinger (1920), such movement can be understood by entanglement mechanisms in the physical sense or by secondary bonds, such as hydrogen bonds, which unlike the primary chemical bonds between polymer chains of the elastic network in rubbers are weak and highly dynamical. One of the early entanglement models goes back to the work in Green and Tobolsky (1946) where it is assumed that such entanglements are steadily created and destroyed. In particular, when a new chain joins the network based on an appearing entanglement, it is assumed that this chain reforms in a stress-free state resulting in a steady decrease of the network stresses in time being characteristic for stress relaxation phenomena. With regard to the equal rate, at which entanglement junctions are assumed to be created and broken, a linear evolution is derived, limiting the applicability to problems with small perturbations from the thermodynamic equilibrium. An extension of the transient network model in Green and Tobolsky (1946) is achieved in Yamamoto (1956, 1957) by accounting for the dependency of the probability of the chain breakage rate on the tension acting in the network and by Lodge (1956) allowing for an anisotropy of the deforming network and the existence of many stress relaxation periods as well as its extension in Bernstein et al. (1963). In Reese and Wriggers (1999) the original model by Green and Tobolsky (1946) is generalized to allow for states away from the thermodynamic equilibrium by the introduction of a stress-free intermediate configuration.

In line with these approaches, the aim of this work is to develop a new micromechanically motivated model for the description of the transient network to describe viscous effects in polymers. The key aspect in the proposed model is the stochastic motion within the viscoelastic part of the network including the re-orientation and stretch relaxation of chain segments. This process is seen as a Brownian motion performed by the chain segment end points within a viscous surrounding idealizing the neighboring chains in the network. Motivated by the description of the movement of non-interacting point particles in a viscous fluid described by the Smoluchowski equation obtained as a generalization of the diffusion equation in Doi and Edwards (1986), this is extended to describe the motion of the chain segment end points governing a change of the distribution of stretch within the subnetwork due to the macrodeformation and internal relaxation of the microstructure. It is further shown that an equivalent tensorial formulation of this micromechanically based model can be derived resulting in evolution equations of the internal variables and closed form expressions of the free energy as in Green and Tobolsky (1946). The thermodynamical consistency comes intrinsically from the micro-mechanical origin which is outlined in detail. This description of the transient network is subsequently combined with the non-affine micro-sphere model developed in Miehe et al. (2004) to represent the elastic ground network and applied to homogeneous and non-homogeneous experimental data sets.

The paper is organized as follows. In Section 2 the basic network mechanisms of finite rubber viscoelasticity of a nearly incompressible solid is summarized which provides the description of the characteristic finite deformation and the basic thermodynamics of the continuum. It is assumed that the response of the rubber-like material can be decomposed into an elastic ground network and a highly mobile viscous subnetwork. For the latter, a micromechanically motivated model is proposed in Section 3. Starting with an entropic spring representation of a single polymer chain based on its equilibrium kinetics, a model for the mobile subnetwork evolution based on the concept of Brownian motion is developed and applied

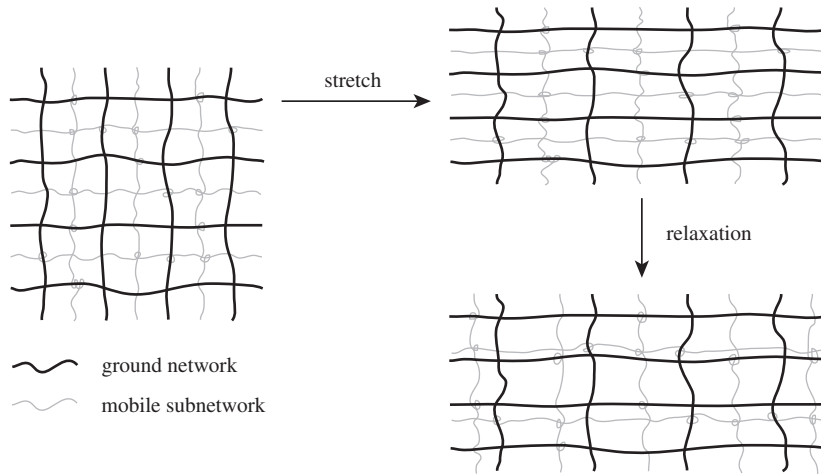


Fig. 1. Network representation of the microscopic response of rubber-like materials. The schematic response of the material decomposed into a strongly cross-linked ground network (representing the elastic response) and a mobile subnetwork (formed by temporary entanglement mechanisms representing the viscous response) is illustrated under an applied arbitrary macrodeformation.

to the network chains whose end points are treated as point particles moving in a viscous surrounding. The final outcome is the flow equation with respect to the stretch probability field that describes the microdeformation of a single subnetwork. In Section 4 an equivalent tensorial representation of the stretch probability evolution is developed which allows for the closed form computation of the macroscopic free energy and the macroscopic viscous overstress. Finally, Section 5 outlines the performance of the model when combined with the non-affine micro-sphere model for the representation of the elastic ground network on a set of homogeneous and non-homogeneous representative problems. The model capacity is evaluated based on comparisons of all tests with available experimental data sets in the literature.

2. Basic network mechanisms of finite rubber viscoelasticity

This section briefly summarizes the resulting constitutive equations of finite rubber viscoelasticity under the basic assumption of the polymer microstructure being assembled by several idealized polymer networks. Motivated by the discussion in Section 1, the response of the rubber-like material is considered to be decomposed into a *ground network* formed by strongly cross-linked macromolecules and a *subnetwork* consisting of highly mobile and based on temporary entanglement mechanisms linked macromolecules. Whereas the ground network is associated with the elastic response of the material, the subnetwork is responsible for the description of the viscous material properties in the form of the appearance of a viscous overstress. An illustration of the resulting viscoelastic behavior is given in Fig. 1 displaying a schematic representation of the individual networks under an applied macrodeformation. Based on such deformation, the ground network stretches and drags the mobile subnetwork along with it. After a sufficient amount of time at a constant deformation, the subnetwork relaxes towards a state at which it produces no viscous overstress. Whereas the elastic ground network can be represented by models such as the eight-chain model developed in Arruda and Boyce (1993a) or the non-affine network model developed in Miehe et al. (2004), among many others, the emphasis of this work is to develop a diffusion-based micromechanically motivated model for the representation of the viscous mobile subnetwork. In fact, the numerical simulations presented in Section 5 make use of the model developed in Miehe et al. (2004) for the representation of the elastic ground network but it should be kept in mind that the developed model of the viscous subnetwork does not rely on a particular model choice for the description of the elastic properties.

Following the geometric setting of finite inelasticity outlined in Miehe (1998), the macroscopic finite rubber viscoelastic response is based on a volumetric-isochoric decomposition, where the isochoric part itself is decomposed into an elastic equilibrium and a viscous overstress response, as it is briefly summarized in this section. To do so, consider a body to be a collection of material points which at time $t \in \mathbb{R}_+$ occupies a spatial configuration $\mathcal{S} \subset \mathbb{R}^{n_{\text{dim}}}$ in terms of the space dimension $1 \leq n_{\text{dim}} \leq 3$. An individual material point of the body at time t is located at position $\mathbf{x} \in \mathcal{S}$. The change of properties of such material point in the body is described relative to a fixed reference configuration $\mathcal{B} \subset \mathbb{R}^{n_{\text{dim}}}$ which for instance can represent the configuration occupied by the body at the instant time t_0 in which the material point is located at position $\mathbf{X} \in \mathcal{B}$. To avoid any explicit reference to the body itself, the non-linear deformation map $\varphi(\mathbf{X}) : \mathbf{X} \mapsto \mathbf{x} = \varphi(\mathbf{X}; t)$ is introduced which maps positions $\mathbf{X} \in \mathcal{B}$ onto positions $\mathbf{x} \in \mathcal{S}$. Key kinematic quantities are the local deformation gradient $\mathbf{F} = \nabla_{\mathbf{X}} \varphi(\mathbf{X}; t)$ representing the linear map between tangent vectors in the reference and the spatial configuration, respectively, where the Jacobian $J = \det \mathbf{F}$ has to satisfy $J > 0$, as well as the covariant Cartesian metric tensors $\mathbf{G} = \delta_{AB}$ and

$\mathbf{g} = \delta_{ab}$ of those configurations written in terms of the Kronecker symbol δ . The boundary value problem of the macroscopic finite viscoelastic problem at hand for the quasi-static case is then governed by the balance of linear momentum

$$\operatorname{div}_{\mathbf{X}}[\boldsymbol{\tau}\mathbf{F}^{-T}] + \bar{\mathbf{B}} = \mathbf{0} \quad (1)$$

written in terms of the divergence operator $\operatorname{div}_{\mathbf{X}}$ with respect to the reference position \mathbf{X} together with prescribed displacement boundary conditions $\boldsymbol{\varphi} = \bar{\boldsymbol{\varphi}}(\mathbf{X}; t)$ on $\partial\mathcal{B}_{\varphi}$ and prescribed traction $[\boldsymbol{\tau}\mathbf{F}^{-T}]\mathbf{N} = \bar{\mathbf{T}}(\mathbf{X}; t)$ on $\partial\mathcal{B}_t$ with outward normal \mathbf{N} . The usual conditions $\partial\mathcal{B}_{\varphi} \cap \partial\mathcal{B}_t = \emptyset$ and $\partial\mathcal{B}_{\varphi} \cup \partial\mathcal{B}_t = \partial\mathcal{B}$ have to hold in each component of the deformation mapping to ensure a well-posed problem. In (1), the prescribed body force field $\bar{\mathbf{B}}$ with respect to the unit volume of the reference configuration as well as the Kirchhoff stress tensor $\boldsymbol{\tau}$ are introduced. The latter is assumed to be a function of the local deformation gradient \mathbf{F} and some internal variables \mathcal{I} responsible for the characterization of the viscous structural changes. The Kirchhoff stress $\boldsymbol{\tau}$ and its associated moduli are given as

$$\boldsymbol{\tau} = 2\partial_{\mathbf{g}}\psi(\mathbf{g}, \mathcal{I}; \mathbf{F}) \quad \text{and} \quad \mathbb{C} = 4\partial_{\mathbf{g}\mathbf{g}}^2\psi(\mathbf{g}, \mathcal{I}; \mathbf{F}) \quad (2)$$

in terms of the macroscopic free energy per unit volume of the reference configuration (Marsden and Hughes, 1983; Miehe, 1998) stored in a deformed polymer network with the requirement of being material frame invariant in the sense that $\psi(\mathbf{g}, \mathcal{I}; \mathbf{Q}\mathbf{F}) = \psi(\mathbf{g}, \mathcal{I}; \mathbf{F})$ for all rotations $\mathbf{Q} \in SO(3)$.

The rubber-like material considered in this work is assumed to be nearly incompressible which motivates a decoupled volumetric-isochoric formulation based on the decomposition of the macroscopic free energy as

$$\psi = U(J) + \bar{\psi}(\mathbf{g}, \mathcal{I}; \bar{\mathbf{F}}) \quad (3)$$

in terms of the volumetric and isochoric contributions, respectively. The numerical simulations presented in Section 5 make use of $U(J) = \kappa(J^2 - 1 - 2\ln J)/4$ for the former contribution. The latter is given in terms of the unimodular part of the deformation gradient defined as $\bar{\mathbf{F}} = J^{-1/3}\mathbf{F}$ which is assumed to drive the deviatoric part $\bar{\boldsymbol{\tau}} = 2\partial_{\mathbf{g}}\bar{\psi}(\mathbf{g}, \mathcal{I}; \bar{\mathbf{F}})$ of the total stresses decomposed into spherical and deviatoric contribution as

$$\boldsymbol{\tau} = p\mathbf{g}^{-1} + \bar{\boldsymbol{\tau}} : \mathbb{P} \quad (4)$$

with $p = JU'(J)$ and the fourth-order deviatoric projection tensor $\mathbb{P}_{cd}^{ab} = [\delta_c^a\delta_d^b + \delta_d^a\delta_c^b]/2 - \delta^{ab}\delta_{cd}/3$. This decomposition carries along into the representation of the moduli \mathbb{C} written in terms of the deviatoric part $\bar{\mathbb{C}} = 4\partial_{\mathbf{g}\mathbf{g}}^2\bar{\psi}(\mathbf{g}, \mathcal{I}; \bar{\mathbf{F}})$ as

$$\mathbb{C} = (p + \kappa)\mathbf{g}^{-1} \otimes \mathbf{g}^{-1} - 2p\mathbb{I} + \mathbb{P}^T : \left[\bar{\mathbb{C}} + \frac{2}{3}(\bar{\boldsymbol{\tau}} : \mathbf{g})\mathbb{I} \right] : \mathbb{P} - \frac{2}{3}(\mathbb{P}^T : \bar{\boldsymbol{\tau}} \otimes \mathbf{g}^{-1} + \mathbf{g}^{-1} \otimes \bar{\boldsymbol{\tau}} : \mathbb{P}) \quad (5)$$

with $\kappa = J^2U''(J)$ and in terms of the fourth-order identity tensor $\mathbb{I}^{abcd} = [\delta^{ac}\delta^{bd} + \delta^{ad}\delta^{bc}]/2$.

To account for the actual behavior of rubber viscoelasticity, the isochoric part of the above model is further decomposed into elastic and viscous parts in accordance with the representation of the polymer network structure into an elastic ground network and a viscous subnetwork illustrated in Fig. 1. In case of s viscous subnetworks which are introduced to obtain a discrete spectrum of relaxation times related to different viscosities $\{\eta_i\}_{i=1}^s$, the isochoric part $\bar{\psi}$ in (3) of the free energy can be additively split into

$$\bar{\psi} = \bar{\psi}^e(\mathbf{g}; \bar{\mathbf{F}}) + \bar{\psi}^v(\mathbf{g}, \mathcal{I}; \bar{\mathbf{F}}) \quad \text{where} \quad \bar{\psi}^v(\mathbf{g}, \mathcal{I}; \bar{\mathbf{F}}) = \sum_{i=1}^s \bar{\psi}_i^v(\mathbf{g}, \mathcal{I}_i; \bar{\mathbf{F}}) \quad (6)$$

is given as a summation over each of the s viscous subnetworks. The corresponding rheological model for such an isochoric response of the material is illustrated in Fig. 2. This further yields to the decomposition of the deviatoric part of the stresses into an elastic equilibrium stress response and a viscous overstress response according to

$$\bar{\boldsymbol{\tau}} = \bar{\boldsymbol{\tau}}^e + \bar{\boldsymbol{\tau}}^v \quad \text{with} \quad \bar{\boldsymbol{\tau}}^e = 2\partial_{\mathbf{g}}\bar{\psi}^e(\mathbf{g}; \bar{\mathbf{F}}) \quad \text{and} \quad \bar{\boldsymbol{\tau}}^v = 2\partial_{\mathbf{g}}\bar{\psi}^v(\mathbf{g}, \mathcal{I}; \bar{\mathbf{F}}). \quad (7)$$

Whereas the response of the elastic equilibrium stress is assumed to be isotropic, resulting in the condition $\bar{\psi}^e(\mathbf{g}; \mathbf{F}\mathbf{Q}) = \bar{\psi}^e(\mathbf{g}; \mathbf{F})\forall \mathbf{Q} \in SO(3)$, a deformation induced anisotropy is provided by the dissipative viscous overstress which is characterized by the evolution of the internal variables \mathcal{I} in time. To obtain a formulation consistent with the second axiom of thermodynamics the local dissipation has to satisfy the inequality

$$\mathcal{D}_{loc} = -\partial_{\mathcal{I}}\bar{\psi} \cdot \dot{\mathcal{I}} = \sum_{i=1}^s \mathcal{D}_{loc,i} \geq 0 \quad \text{where} \quad \mathcal{D}_{loc,i} = -\partial_{\mathcal{I}_i}\bar{\psi}_i \cdot \dot{\mathcal{I}}_i. \quad (8)$$

After presenting a brief overview of the basic network mechanisms of rubber viscoelasticity and its incorporation into standard finite rubber viscoelasticity, the remaining part of the work is concerned with the development of a diffusion-based, from a microscopic point of view physically motivated, transient network model resulting in expressions for the viscous part $\bar{\psi}^v$ of the isochoric free energy as well as for the viscous overstress response $\bar{\boldsymbol{\tau}}^v$. Whereas Section 3 will develop the diffusion-based micromechanical polymer model, its incorporation into the macroscopic framework above is

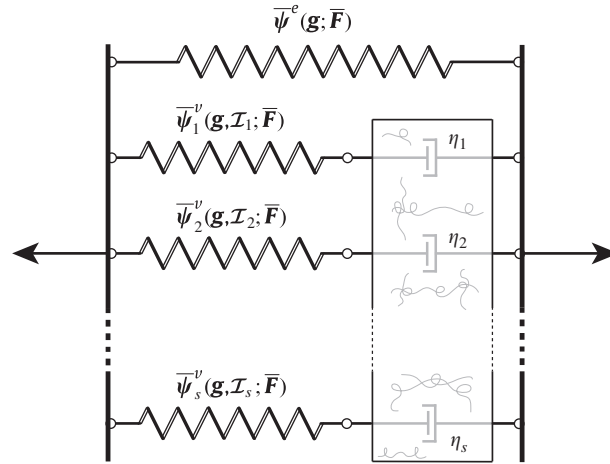


Fig. 2. Macroscopic representation of finite rubber viscoelasticity. The Maxwellian type rheological model of the isochoric response of the material consists of a single elastic branch representing the elastic ground network in Fig. 1 as well as s viscous branches each of them representing a single mobile viscous subnetwork in Fig. 1.

achieved in Section 4 and finally evaluated through representative numerical simulations in Section 5 based on homogeneous and non-homogeneous tests.

3. Microscopic formulation of the diffusion-based transient network model

In this section a micromechanical model for the description of the polymer chain movement is developed. The model makes use of the concept of diffusion to approximate the time evolution of the probability density function associated with the end-to-end vector of the individual chain segments undergoing a Brownian movement. The application of statistical methods for the description of micromechanical states of rubber-like polymers is justified by the enormous number of conformations in time based on the rotation of chemical bonds such materials may undergo. In Section 3.1 the Gaussian statistics of a single chain is briefly reviewed. To account for viscoelastic phenomena in polymers related to the dissipation of mechanical work, the framework of non-equilibrium thermodynamics is introduced in Section 3.2 when describing a diffusion-based process of the Brownian motion of non-interacting point particles. This framework is extended in Section 3.3 to describe the Brownian motion of polymer chains representing the core part of the developed micromechanical polymer model in this section.

3.1. Gaussian statistics of a single polymer chain

Following the classical work in Kuhn (1934, 1936) or the more recent contribution of Treloar (1975) or Doi and Edwards (1986), in this section a brief review of the statistics of a single polymer chain is provided in the form of the most simple case of a *freely jointed model*. The model, which already captures many of the characteristic properties of a single polymer chain, rests upon the assumption that such chain consists of N links, each of length b , whose orientations are assumed to be random and independent of each other. The conformation of such freely jointed chain is determined either by $(N + 1)$ position vectors $\{\mathbf{r}_n\}_{n=0}^N$ of the joints including the two end points or alternatively by a set of N independent bond vectors $\{\mathbf{b}_n\}_{n=1}^N$ with $\mathbf{b}_n = \mathbf{r}_n - \mathbf{r}_{n-1}$ for $n = 1, \dots, N$. Viewing the chain as a statistical system, the probability of a particular chain conformation $\{\mathbf{b}_n\}_{n=1}^N$ can be computed by

$$p(\{\mathbf{b}_n\}_{n=1}^N) = \prod_{n=1}^N p(\mathbf{b}_n) \quad \text{with} \quad p(\mathbf{b}_n) = \frac{1}{4\pi b^2} \delta(|\mathbf{b}_n| - b) \tag{9}$$

as the product of the isotropic distribution of the individual random bond vectors with fixed length b expressed in \mathbb{R}^3 by the single-layer potential $p(\mathbf{b}_n)$ given in terms of $|\mathbf{b}_n| = \sqrt{\mathbf{b}_n \cdot \mathbf{b}_n}$ and normalized according to the condition $\int_{\mathbb{R}^3} p(\mathbf{b}_n) d\mathbf{b}_n = 1$. The size of the polymer chain can then be characterized by the end-to-end vector \mathbf{r} defined as $\mathbf{r} = \mathbf{r}_N - \mathbf{r}_0 = \sum_{n=1}^N \mathbf{b}_n$ with the corresponding mean value $\langle \mathbf{r} \rangle = \sum_{n=1}^N \langle \mathbf{b}_n \rangle = \mathbf{0}$ and mean-square value $\langle \mathbf{r}^2 \rangle = \sum_{n,m=1}^N \langle \mathbf{b}_n \cdot \mathbf{b}_m \rangle = Nb^2$, for sufficiently large N . Here, $\langle \bullet \rangle$ denotes the mean value of a random quantity (\bullet) that is computed as an integral over the probability space as

$$\langle \bullet \rangle = \int (\bullet) d\{\mathbf{b}_n\}_{n=1}^N. \tag{10}$$

The above mean values do not provide sufficient information to describe the statistical system of the freely jointed model. What is required is the knowledge about the corresponding statistical distribution of the end-to-end vector \mathbf{r} given as

$$p(\mathbf{r}) = \int p(\{\mathbf{b}_n\}_{n=1}^N) \delta\left(\mathbf{r} - \sum_{n=1}^N \mathbf{b}_n\right) d\{\mathbf{b}_n\}_{n=1}^N = \left(\frac{3}{2\pi r_0^2}\right)^{3/2} \exp\left[-\frac{3r^2}{2r_0^2}\right] \quad (11)$$

whose solution is given (see Doi and Edwards (1986) for a detailed derivation) in terms of $r = |\mathbf{r}|$ and $r_0^2 = \langle r^2 \rangle$ in the form of a Gaussian distribution. It is emphasized that as a result of the central limit theorem in statistics, for $N \gg 1$ the obtained result (11) of the freely jointed model holds even for a more general class of models with the only difference of the actual bond length b being replaced by an effective counterpart (Doi and Edwards, 1986). On the other hand, the solution obtained in (11) has the non-physical feature that the probability of finding end-to-end vectors with $r > Nb$, where Nb represents the length of a fully extended chain, is non-zero. Nonetheless, it provides a good estimate for models in which highly stretched states of the polymer chains do not play an important role, as it is the case for the diffusion-based micromechanical polymer model developed in this section for the representation of the mobile viscous subnetworks introduced in Section 2.

The distribution $p(\mathbf{r})$ in (11) can be understood as a measure of the number of conformations of a chain and can, therefore, be directly linked to the entropy. Considering a thermodynamical system of a polymer chain with the constrained position of the ends one can postulate the entropy \mathcal{S} in the form of Boltzmann's relation

$$\mathcal{S}(\mathbf{r}) = k_B \ln p(\mathbf{r}) = -\frac{3}{2} k_B \frac{r^2}{r_0^2} + \text{terms independent of } \mathbf{r} \quad (12)$$

where k_B is the Boltzmann constant. When rotations about the bonds in the molecular polymer chain are considered to be unrestricted, the internal energy will remain the same for all conformations (Treloar, 1975) so that the Helmholtz free energy can be solely computed based on the entropy in (12) as

$$\mathcal{A}(\mathbf{r}) = -\theta \mathcal{S}(\mathbf{r}) = \frac{3}{2} k_B \theta \frac{r^2}{r_0^2} + \text{terms independent of } \mathbf{r} \quad (13)$$

in terms of the known temperature θ of the polymer. In analogy to existing bead-spring models (Bird et al., 1977), this viewpoint motivates the interpretation of a polymer chain with fixed end points and different conformations in between those by an entropic spring expressing the average response from the thermal motion of the chain segments. The thermodynamic force acting on the fixed ends of such spring then becomes

$$F_r = \frac{\partial \mathcal{A}}{\partial r} = 3k_B \theta \frac{r}{r_0^2}. \quad (14)$$

The simplified theory discussed in this section neglects possible temporary constraints like bonding or detachment of polymer chain segments leading to time-dependent phenomena such as viscoelasticity. The incorporation of such effects is achieved within the framework of non-equilibrium thermodynamics in the subsequent Section 3.2.

3.2. Brownian motion of non-interacting point particles

The incorporation of viscoelasticity as a time-dependent phenomena of polymers related to the dissipation of mechanical work on the micromechanical level is achieved by the development of a model which treats the viscoelastic relaxation of the microstructure as a diffusion-based process allowing for the incorporation of the formalism of Brownian motion. Following the phenomenological approach in Doi and Edwards (1986), the Brownian motion can be interpreted as a stochastic process that is governed by known macroscopic laws applied to microscopic objects. Such a treatment is restricted to time- and length-scales larger than those characteristic of equilibrium thermal oscillations. The resulting phenomenological evolution equation in the form of the *Smoluchowski equation* is derived from the generalization of the diffusion equation and can be related to the thermodynamics of irreversible processes. To allow for a concise derivation of the Smoluchowski equation, in the following the Brownian motion of non-interacting point particles is restricted to translational degrees of freedom.

To do so, consider a system with a large number of point particles submerged in a viscous medium as it is illustrated on the left of Fig. 3. The phenomena of diffusion can be observed in such a system when the distribution of particles in the medium is not uniform resulting in a flux which is proportional to the spatial gradient of the concentration of particles. The microscopic origin of the macroscopically observed flux is motivated in Doi and Edwards (1986) by the random thermal motion of the particles in the sense that in case of a non-uniform concentration, the number of particles flowing from regions of higher concentration to regions of lower concentration surpasses the number of particles moving in the opposite direction.

To describe this process, consider the probability of finding a particle in a certain state governed by its position \mathbf{x} at a certain time t expressed by the probability function $p(\mathbf{x}, t)$ which can be viewed as the concentration of particles $c(\mathbf{x}, t)$ scaled to the total number of particles n as $c(\mathbf{x}, t) = np(\mathbf{x}, t)$. This distribution evolves in time based on the continuity

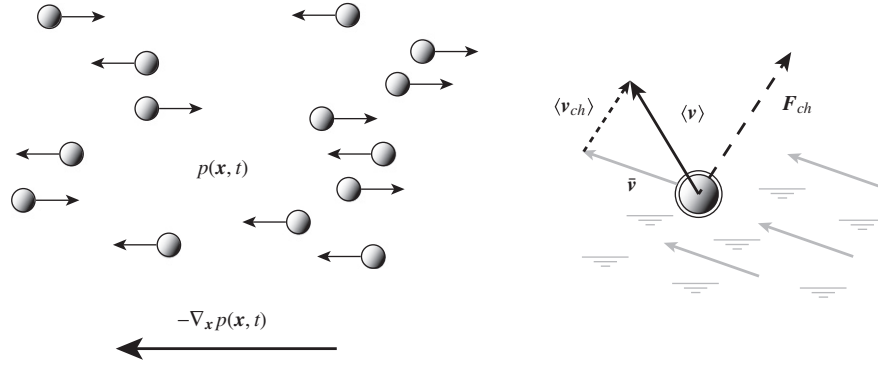


Fig. 3. Brownian motion of non-interacting point particles. A non-uniform distribution of particles results in a flow proportional to the spatial gradient of particles from regions of high concentration to regions of low concentration as shown on the left. The right figure shows the resulting average velocity $\langle \mathbf{v} \rangle$ of point particles submerged in a, with velocity $\bar{\mathbf{v}}$, moving viscous medium.

equation

$$\partial_t p(\mathbf{x}, t) = -\text{div}_{\mathbf{x}} \mathbf{h}(\mathbf{x}, t) \tag{15}$$

where $\mathbf{h}(\mathbf{x}, t)$ consists of the flux $\mathbf{h}_{ch}(\mathbf{x}, t)$ induced by the thermal motion of the particles and an additional flux arising from the motion of the surrounding viscous medium. The former is given as

$$\mathbf{h}_{ch}(\mathbf{x}, t) = -p(\mathbf{x}, t) \frac{1}{\eta} \nabla_{\mathbf{x}} U_{ch} \quad \text{where} \quad U_{ch}(\mathbf{x}, t) = k_B \theta \ln p(\mathbf{x}, t) + U(\mathbf{x}) \tag{16}$$

is called the chemical potential resulting in a flux contribution coming from the thermal motion of the particles in the presence of a non-uniform concentration $-D \nabla_{\mathbf{x}} p(\mathbf{x}, t)$ in terms of the diffusion constant $D = k_B \theta / \eta$ with $\eta > 0$ as the viscosity and the additional contribution $-p(\mathbf{x}, t) / \eta \nabla_{\mathbf{x}} U(\mathbf{x})$ induced by the presence of a stationary potential $U(\mathbf{x})$. The chemical potential $U_{ch}(\mathbf{x}, t)$ in (16) expresses the energy of a certain particle at state \mathbf{x} and time t so that the resulting evolution of the particle distribution based on (15) can be interpreted as the motion of particles from states with high energy towards states with lower energy. This motion is driven by a chemical force \mathbf{F}_{ch} that in addition determines the average velocity $\langle \mathbf{v}_{ch} \rangle$ of the particles relative to the viscous medium. Both are given in terms of the chemical potential as

$$\mathbf{F}_{ch} = -\nabla_{\mathbf{x}} U_{ch} \quad \text{and} \quad \langle \mathbf{v}_{ch} \rangle = \frac{1}{\eta} \mathbf{F}_{ch} = -\frac{1}{\eta} \nabla_{\mathbf{x}} U_{ch} \tag{17}$$

so that the flux in (16) is found as $\mathbf{h}_{ch}(\mathbf{x}, t) = p(\mathbf{x}, t) \langle \mathbf{v}_{ch} \rangle$. The second contribution to the flux $\mathbf{h}(\mathbf{x}, t)$ in (15) comes from the macroscopic motion of the viscous medium surrounding and influencing the flow of the particles. To account for such movement one has to add the contribution of the macroscopic velocity $\bar{\mathbf{v}}(\mathbf{x}, t)$ to the average particle velocity $\langle \mathbf{v}_{ch} \rangle$ arising from the chemical potential resulting in a total average velocity $\langle \mathbf{v} \rangle$ and a total flux $\mathbf{h}(\mathbf{x}, t)$ given as

$$\langle \mathbf{v} \rangle = \bar{\mathbf{v}} + \langle \mathbf{v}_{ch} \rangle \quad \text{and} \quad \mathbf{h}(\mathbf{x}, t) = p(\mathbf{x}, t) \langle \mathbf{v} \rangle \tag{18}$$

respectively. Insertion of these expressions into (15) leads to the final form of the Smoluchowski equation describing the Brownian motion of particles subjected to an external potential force field in a moving viscous medium as

$$\partial_t p(\mathbf{x}, t) = -\text{div}_{\mathbf{x}} [p(\mathbf{x}, t) \bar{\mathbf{v}}] + \frac{1}{\eta} \text{div}_{\mathbf{x}} [p(\mathbf{x}, t) \nabla_{\mathbf{x}} (k_B \theta \ln p(\mathbf{x}, t) + U(\mathbf{x}))]. \tag{19}$$

Remark 1.

(a) The Smoluchowski equation (19) is dissipative which can be observed based on the introduction of

$$\mathcal{A}(p) = n \int p(\mathbf{x}, t) U_{ch} |d\mathbf{x}| \tag{20}$$

representing the dynamic free energy of the thermodynamic system of Brownian particles (Doi and Edwards, 1986) in terms of the distribution $p(\mathbf{x}, t)$ summing up the chemical potential U_{ch} over all the n particles in the system. For the case of a non-moving viscous surrounding ($\bar{\mathbf{v}} = \mathbf{0}$) under isothermal conditions ($\theta = \text{constant}$) together with using (16), (19), $\int \partial_t p |d\mathbf{x}| = 0$ and integration by parts, where the contribution of the boundary integral is assumed to vanish, one can show that the time change of \mathcal{A} , given as

$$\frac{d\mathcal{A}}{dt} = -n \int \frac{\eta}{p(\mathbf{x}, t)} \mathbf{h}_{ch}(\mathbf{x}, t) \cdot \mathbf{h}_{ch}(\mathbf{x}, t) |d\mathbf{x}| \leq 0 \tag{21}$$

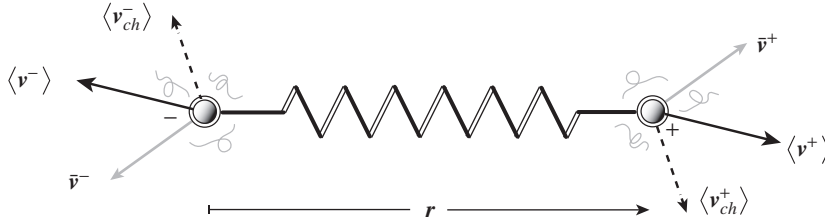


Fig. 4. Lagrangian description of the Brownian motion of flexible polymer chains. The polymer chain with end-to-end vector \mathbf{r} is modeled as an entropic spring and placed into a viscous moving surrounding representing the remaining polymer network where the viscosity is concentrated at the chain end points. The resulting relative movement of these end points is described by the kinetic relation (26).

is negative. The inequality emphasizes the fact that diffusion drives the relaxation of the system towards the equilibrium state where $\mathbf{h}_{ch}(\mathbf{x}, t)$ given in (16) is responsible for the resulting dissipative flow.

(b) The equilibrium state is attained in the absence of macroscopic flow of the surrounding medium for a vanishing flux $\mathbf{h}_{ch} = \mathbf{0}$ so that $\nabla_{\mathbf{x}} U_{ch} = \mathbf{0}$ results in the equilibrium distribution

$$p_{eq}(\mathbf{x}) = \exp\left[-\frac{U(\mathbf{x})}{k_B\theta}\right] / \int \exp\left[-\frac{U(\mathbf{x})}{k_B\theta}\right] |d\mathbf{x}| \tag{22}$$

where the denominator results from the normalization condition $\int p_{eq} |d\mathbf{x}| = 1$. In the equilibrium state (22) the inequality in (21) becomes an equality with vanishing change of the free energy in time.

3.3. Brownian motion of flexible polymer chains

In this section the presented model of the previous section is extended to describe the Brownian motion of flexible polymer chains. Analogous to the point particles in Section 3.2, the proposed model assumes that the polymer chains are immersed into a viscous medium representing the surrounding polymer network. Contrary to the previous section where the state of the individual particles was described by their position \mathbf{x} , the state of the polymer chain is described in terms of the in Section 3.1 introduced end-to-end vector \mathbf{r} or analogously in terms of the newly introduced vector $\lambda = \mathbf{r}/r_0$ as a measure of the rotation and stretch of the chain. The state of the overall thermodynamic system consisting of a large number of such chains in the vicinity of a material point can then be described by the distribution $p(\lambda, t)$ in \mathbb{R}^3 .

Each polymer chain is now modeled as an entropic spring with the energy given based on (13) as

$$U(\lambda) = \frac{3}{2}k_B\theta\lambda^2 + \text{terms independent of } \lambda \tag{23}$$

where $\lambda = |\lambda| = r/r_0$. It is further assumed that the viscosity is concentrated at the ends of the polymer chains, where we refer as the $-$ and the $+$ end the starting and the end point of the end-to-end vector \mathbf{r} , respectively. This results in the kinematic relation illustrated in Fig. 4 where on average the two end points are moving according to

$$\langle \mathbf{v}^\pm \rangle = \bar{\mathbf{v}}^\pm + \langle \mathbf{v}_{ch}^\pm \rangle \tag{24}$$

in terms of the velocity $\bar{\mathbf{v}}^\pm$ resulting from the motion of the surrounding viscous medium and the motion of the thermally active polymer chains $\langle \mathbf{v}_{ch}^\pm \rangle$ given as

$$\bar{\mathbf{v}}^\pm = \pm \frac{\mathbf{l}\mathbf{r}}{2} = \pm \frac{r_0\mathbf{l}\lambda}{2} \quad \text{and} \quad \langle \mathbf{v}_{ch}^\pm \rangle = \mp \frac{1}{\eta} \nabla_{\mathbf{r}} U_{ch}(\mathbf{r}, t) = \mp \frac{1}{\eta r_0} \nabla_\lambda U_{ch}(\lambda, t) \tag{25}$$

respectively. The first part $\bar{\mathbf{v}}^\pm$ of the end point velocities in (24) corresponds to the changes in the mobile network following the macroscopic velocity gradient $\mathbf{l} = \dot{\mathbf{F}}\mathbf{F}^{-1}$ with \mathbf{F} being the deformation gradient. The second part $\langle \mathbf{v}_{ch}^\pm \rangle = \mathbf{F}_{ch}^\pm / \eta$ introduces the diffusion-based average motion of chain segments relative to the viscous medium under the action of the chemical forces $\mathbf{F}_{ch}^\pm = \mp \nabla_{\mathbf{r}} U_{ch} = \mp \nabla_\lambda U_{ch} / r_0$ conjugate to the length r of the spring or its stretch λ drawing their ends. Summing up the velocities of the end points one derives the average transient change of the end-to-end vector $\langle \dot{\mathbf{r}} \rangle = \langle \mathbf{v}^+ \rangle - \langle \mathbf{v}^- \rangle$ which can be expressed in terms of the evolution of the stretch as

$$\langle \dot{\lambda} \rangle = \mathbf{l}\lambda - D^\lambda \nabla_\lambda \left[\ln p(\lambda, t) + \frac{3}{2}\lambda^2 \right] \quad \text{where} \quad D^\lambda = \frac{2k_B\theta}{\eta r_0^2}. \tag{26}$$

The result in (26) makes use of the chemical potential $U_{ch}(\lambda, t)$ defined in stretch space analogous to (16) as

$$U_{ch}(\lambda, t) = k_B\theta \ln p(\lambda, t) + \frac{3}{2}k_B\theta\lambda^2. \tag{27}$$

The resulting diffusion process of the polymer chains can hence be interpreted as re-orientation and re-distribution of polymer chain stretches which, in analogy to (15), can be described as

$$\partial_t p(\lambda, t) = -\text{div}_\lambda [p(\lambda, t) \langle \dot{\lambda} \rangle] = -\text{div}_\lambda (\mathbf{h}_{rev} + \mathbf{h}_{dis}). \tag{28}$$

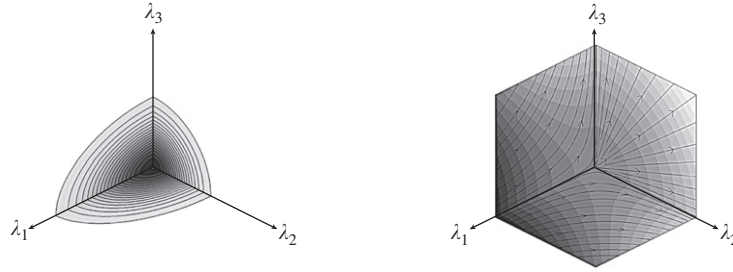


Fig. 5. Eulerian description of the Brownian motion of flexible polymer chains. A perturbation of the probability distribution $p(\lambda, t)$ due to an instantaneous macroscopic deformation schematically shown on the left results in an inhomogeneity of the chemical potential field $U_{ch}(\lambda, t)$ and a resulting flow based on (29) leading to a change of probability according to the Smoluchowski equation in (28).

The two equations (26) and (28) can be viewed as the Lagrangian and the Eulerian description of the microscopic diffusional motion. Whereas the former follows a particular chain stretch and tracks the average velocity $\langle \dot{\lambda} \rangle$ of its endpoints, the resulting Smoluchowski equation in (28) is concerned with the change of the probability of a certain state λ in time.

One can further observe both, a reversible and dissipative part of the evolution equation for the probability distribution in (28) in terms of the corresponding fluxes defined as

$$\mathbf{h}_{rev}(\lambda, t) = p(\lambda, t)\mathbf{l}\dot{\lambda} \quad \text{and} \quad \mathbf{h}_{dis}(\lambda, t) = -D^2 p(\lambda, t)\nabla_{\lambda}[\ln p(\lambda, t) + \frac{3}{2}\lambda^2] \quad (29)$$

respectively. The reversible part arises due to the motion of the polymer chain in accordance with the surrounding macromedium, whereas the dissipative part results from the diffusion and stretch relaxation. The dependence of the latter contribution on the mean-square length r_0 through D^2 emphasizes further the influence of the chain length on the diffusion process. The shorter the chain, the higher is its mobility.

Remark 2.

- (a) The dynamic free energy of the thermodynamic system is again obtained as an integral of the chemical potential (27) over all the possible states λ in the stretch space represented by \mathbb{R}^3 as

$$\mathcal{A} = n \int_{\mathbb{R}^3} p(\lambda, t) U_{ch} |d\lambda| = nk_B \theta \int_{\mathbb{R}^3} p(\lambda, t) [\ln p(\lambda, t) + \frac{3}{2}\lambda^2] |d\lambda| \quad (30)$$

where n represents now the number of polymer chains in the system. For the case of a non-moving viscous surrounding ($\mathbf{l} = \mathbf{0}$) under isothermal conditions ($\theta = \text{constant}$) it can be further shown that the free energy is again decreasing in time as already outlined in Remark 1 for the point particles.

- (b) The equilibrium state is characterized by a natural unperturbed state of the end-to-end vector probability

$$p_{eq}(\lambda) = \exp\left[-\frac{3}{2}\lambda^2\right] / \int_{\mathbb{R}^3} \exp\left[-\frac{3}{2}\lambda^2\right] |d\lambda| = \left(\frac{3}{2\pi}\right)^{3/2} \exp\left[-\frac{3}{2}\lambda^2\right] \quad (31)$$

representing a Gaussian bell-shaped distribution for which the flux \mathbf{h}_{dis} in (29) vanishes.

The resulting mechanism of viscoelasticity can now be understood by considering a macroscopic motion defined by the macrodeformation represented in terms of the velocity gradient \mathbf{l} which pulls the system out of equilibrium and deforms the initial distribution (31) as depicted on the left of Fig. 5. This results in a change in the chemical potential U_{ch} making it inhomogeneous so that the chemical force \mathbf{F}_{ch} , driving the diffusion process, develops. When the macrodeformation freezes, meaning that it remains constant for a sufficiently long time, this process will return the system to the unperturbed state based on a diffusional flow depicted on the right of Fig. 5 in which mechanical work will be dissipated.

4. Macroscopic formulation of the diffusion-based transient network model

The goal of this section is to embed the diffusion-based micromechanical polymer model developed in the previous Section 3 into the framework of finite rubber viscoelasticity by the construction of closed form expressions for the viscous part of the isochoric free energy $\bar{\psi}^v$ in (6) as well as the corresponding viscous overstresses $\bar{\tau}^v$ in (7) for a single viscous subnetwork illustrated in Fig. 2.

Above, the microscopic model of Section 3.2 is treated as a thermodynamic system of Brownian point particles which is extended in Section 3.3 towards the description of the Brownian motion of flexible polymer chains. It is shown that the temporary state of such a system is described by the probability function $p(\lambda)$ whose evolution in time is driven by (28) in the form of the Smoluchowski equation. Solving this parabolic differential equation directly does not allow for solutions of the free energy $\bar{\psi}^v$ or the viscous overstress $\bar{\tau}^v$ which can be expressed in closed form. It is for this reason that a particular

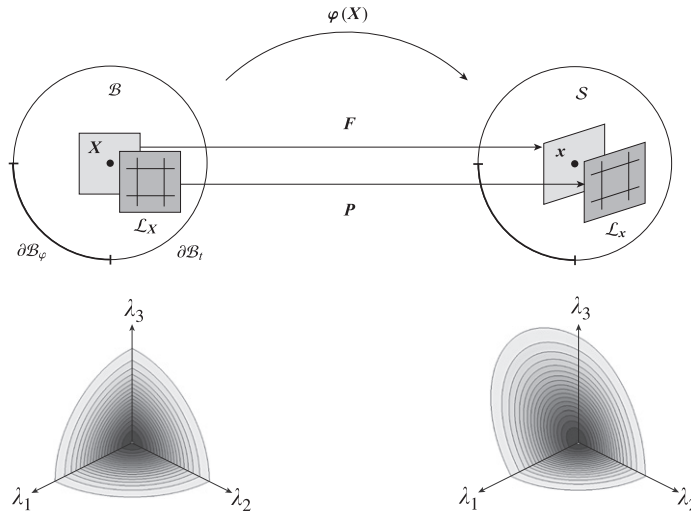


Fig. 6. Tensorial representation of the probability function evolution. The stretch spaces \mathcal{L}_X and \mathcal{L}_x connected to a material point with position \mathbf{X} and \mathbf{x} in the reference and the current configuration and its relation through the microdeformation map \mathbf{P} is outlined in the top figure. The figure below schematically shows the change in probability $p(\lambda)$ in \mathcal{L}_x starting from the equilibrium distribution $P(\Lambda)$ in \mathcal{L}_X due to some arbitrary microdeformation \mathbf{P} .

choice for the change of the probability function $p(\lambda)$ is assumed in Section 4.1 in the form of a tensorial representation of its evolution resulting in the desired closed form solutions of these quantities. Section 4.2 then derives these closed form solutions of the viscous part of the isochoric free energy as well as for the viscous overstress and gives a proof of the satisfaction of the thermodynamic consistency of the proposed model. Finally, Section 4.3 summarizes the algorithmic representation and implementation of the model.

4.1. Tensorial representation of the probability function evolution

In the following a tensorial representation of the evolution of the probability function is assumed, which allows for a closed form representation of the macroscopic quantities within the finite rubber viscoelasticity model. In particular, this section outlines how the Smoluchowski equation (28) can equivalently be described based on an ordinary differential equation in one tensorial quantity.

To do so, use is made of the representation of changes of the solids macroscopic properties in the current configuration \mathcal{S} with respect to a reference configuration \mathcal{B} , as it is outlined briefly in Section 2, where the deformation gradient \mathbf{F} acts as the linear map between tangent vectors of those spaces. The property of interest in this setting is now given by the probability function $p(\lambda) : \mathcal{L}_x \rightarrow \mathbb{R}$ where $\mathcal{L}_x = \mathbb{R}^3$ is the stretch space connected locally to a material point with position \mathbf{x} in the current configuration \mathcal{S} . Its evolution is described with respect to an introduced referential probability function P living in a stretch space $\mathcal{L}_X = \mathbb{R}^3$ connected to a material point with position \mathbf{X} in the reference configuration \mathcal{B} . This initial probability function is assumed to be given as

$$P(\Lambda) = \left(\frac{3}{2\pi}\right)^{3/2} \exp\left[-\frac{3}{2}\Lambda^2\right] \tag{32}$$

in the form of a Gaussian distribution in terms of the norm Λ of the referential stretch vector Λ . The two stretch spaces are linked by a *microdeformation map*

$$\mathbf{P} : \begin{cases} \mathcal{L}_X \rightarrow \mathcal{L}_x \\ \Lambda \mapsto \lambda = \mathbf{P}\Lambda \end{cases} \tag{33}$$

as it is illustrated in Fig. 6. The evolution of $p(\lambda)$ with respect to $P(\Lambda)$ is then assumed to depend on this microdeformation map in (33) based on the relation

$$p(\lambda) = \frac{1}{\det \mathbf{P}} P(\Lambda). \tag{34}$$

A schematic representation of the relation between those probability functions is outlined in Fig. 6. It shows the change of the probability function $p(\lambda)$ of a point \mathbf{x} in the current configuration based on the application of an arbitrary microdeformation map \mathbf{P} when starting from an unperturbed probability function $P(\Lambda)$ of the same material point \mathbf{X} in the reference configuration. It is noted that the spaces \mathcal{L}_X and \mathcal{L}_x contain microscopic objects such as their corresponding stretch vectors Λ and λ , respectively. Even though those objects are not considered within an infinitesimal setting, they belong to such a small scale that they can interfere with objects from the tangent spaces of the body's configurations \mathcal{B} and

S. Such property is exploited in Section 3.3 by adding the macrovelocity $\bar{\mathbf{v}}^\pm$ to the microvelocities $\langle \mathbf{v}_{ch}^\pm \rangle$ in (24). Moreover they share the metric tensors \mathbf{G} and \mathbf{g} of the tangential spaces introduced in Section 2.

The microscopic origin of the cause for the evolution of the stretch probability $p(\lambda)$ is given by the chemical potential (27) which, based on (32) and (34), takes the form

$$U_{ch}(\lambda) = k_B \theta \left\{ -\frac{3}{2} A^2 - \ln(\det \mathbf{P}) + \frac{3}{2} \lambda^2 \right\} \quad (35)$$

when neglecting expressions constant in λ . The resulting expression in (35) is quadratic in terms of the stretches $\lambda = |\lambda|_{\mathbf{g}} = \sqrt{\lambda \cdot \mathbf{g} \lambda}$ and $A = |\mathbf{A}|_{\mathbf{G}} = \sqrt{\mathbf{A} \cdot \mathbf{G} \mathbf{A}} = \sqrt{\lambda \cdot \mathbf{P}^{-T} \mathbf{G} \mathbf{P}^{-1} \lambda}$. This result allows for the computation of the average rate of change of the stretch vector based on (26) as

$$\langle \dot{\lambda} \rangle = \mathbf{I} \lambda - 3D^\lambda \mathbf{g}^{-1} (-\mathbf{P}^{-T} \mathbf{G} \mathbf{P}^{-1} \lambda + \mathbf{g} \lambda) \quad (36)$$

written now in terms of the microdeformation map \mathbf{P} of (33). The obtained expression in (36) is linear in λ from which it follows that the relation between the probability functions in (34) is preserved, validating the equivalent representation of the Smoluchowski equation in terms of the tensorial representation introduced above. Insertion of (33) into (36) results in

$$\dot{\mathbf{P}} \mathbf{P}^{-1} \lambda = [\mathbf{I} - 3D^\lambda \mathbf{g}^{-1} (-\mathbf{P}^{-T} \mathbf{G} \mathbf{P}^{-1} + \mathbf{g})] \lambda \quad (37)$$

which results, after multiplying with the metric tensor \mathbf{g} from the left and after expressing the velocity gradient \mathbf{I} in terms of the isochoric part of the deformation gradient $\bar{\mathbf{F}}$, in the evolution equation for the tensorial microdeformation map \mathbf{P} as

$$\mathbf{g} \dot{\mathbf{P}} \mathbf{P}^{-1} = \mathbf{g} \bar{\mathbf{F}} \bar{\mathbf{F}}^{-1} - 3D^\lambda (-\mathbf{P}^{-T} \mathbf{G} \mathbf{P}^{-1} + \mathbf{g}). \quad (38)$$

This evolution equation consists of a reversible part related to the macrodeformation represented by $\mathbf{I} = \dot{\bar{\mathbf{F}}} \bar{\mathbf{F}}^{-1}$ and a dissipative part due to the diffusion-based mechanism introduced in Section 3 in terms of the diffusion coefficient D^λ defined in (26). To avoid a dependence of the evolution of the microdeformation map on the macrodeformation, the tensor \mathbf{P} is split into $\mathbf{P} = \bar{\mathbf{F}} \mathbf{P}_X$ in terms of a newly introduced tensorial quantity $\mathbf{P}_X : \mathcal{L}_X \rightarrow \mathcal{L}_X$ denoted as *pre-deformation map*. The corresponding evolution equation can then be derived from (38) as

$$\dot{\mathbf{P}}_X = 3D^\lambda (\bar{\mathbf{F}}^{-1} \mathbf{g}^{-1} \bar{\mathbf{F}}^{-T} \mathbf{P}_X^T \mathbf{G} - \mathbf{P}_X) \quad (39)$$

solely in terms of microscopic object. Since \mathbf{P}_X in general is a non-symmetric tensor, it includes both, information with regard to *pre-stretch* and *pre-rotation* where the latter does not influence the overall free energy and can, therefore, be excluded from the formulation. This is achieved by the introduction of the symmetric tensorial quantity

$$\mathbf{A} = \mathbf{P}_X \mathbf{G}^{-1} \mathbf{P}_X^T \quad (40)$$

that contains all the required information about the microdeformation of the viscoelastic subnetwork. The evolution of that expression can be obtained by plugging (40) into (39) which results in

$$\dot{\mathbf{A}} = \frac{1}{\tau} (\bar{\mathbf{C}}^{-1} - \mathbf{A}) \quad \text{with} \quad \frac{1}{\tau} = 6D^\lambda \quad (41)$$

an evolution equation which surprisingly has a form close to existing models of finite viscoelasticity. Conduct Remark 3 with regard to a further discussion on similarities with already existing models in the literature. The developed evolution equation in (41) allows for an interpretation of the introduced symmetric tensor \mathbf{A} in (40) as some intermediate metric whose change is driven by its difference when compared to the referential metric $\bar{\mathbf{C}}^{-1}$ where $\bar{\mathbf{C}} = \bar{\mathbf{F}}^T \mathbf{g} \bar{\mathbf{F}}$ is the isochoric part of the right Cauchy Green tensor. An equilibrium state is obtained as soon as those two metric tensors coincide for which a fully relaxed subnetwork is expected.

4.2. Isochoric viscous free energy and viscous overstress expressions

The goal of this section is to show that the tensorial representation of the change in the probability function determined by (41) allows further for a closed form expression of the viscous part of the isochoric free energy and the viscous overstress.

In particular, the macroscopic free energy is obtained by homogenization of the free energy of the thermodynamic system in (30) for the particular form $p(\lambda)$ and $U_{ch}(\lambda)$ in (34) and (35) over the stretch space as

$$\bar{\psi}^v = n \int_{\mathcal{L}_X} p(\lambda) U_{ch}(\lambda) |d\lambda| = \mu^v \left[\int_{\mathcal{L}_X} P(\mathbf{A}) \left(-\frac{3}{2} A^2 + \frac{3}{2} \lambda^2 \right) |d\mathbf{A}| - \ln(\det \mathbf{P}) \right] \quad (42)$$

where the constant terms are neglected in the latter expression and the viscous overstress moduli is introduced as $\mu^v = nk_B \theta$. The integration over \mathcal{L}_X can then be computed by separating the integration over the stretch value A and the stretch orientation $\mathbf{T} = \mathbf{A}/A \in S^2$ living on the 2-sphere S^2 . This leads to $\lambda^2 = \lambda \cdot \mathbf{g} \lambda = A^2 \mathbf{T} \cdot \mathbf{P}^T \mathbf{g} \mathbf{P} \mathbf{T}$ and $|d\mathbf{A}| = A^2 dA |d\mathbf{T}|$ so that the integral in (42) becomes

$$\int_{\mathcal{L}_X} P(\mathbf{A}) \left(-\frac{3}{2} A^2 + \frac{3}{2} \lambda^2 \right) |d\mathbf{A}| = \frac{3}{2} \int_0^\infty P(\mathbf{A}) A^4 dA \cdot \int_{S^2} (\mathbf{T} \cdot \mathbf{P}^T \mathbf{g} \mathbf{P} \mathbf{T} - 1) |d\mathbf{T}|. \quad (43)$$

Using (32) it can easily be shown that the first integral on the right hand side of (43) becomes

$$\int_0^\infty P(\mathbf{A}) A^4 dA = \frac{1}{4\pi} = \frac{1}{|S^2|}. \quad (44)$$

The identity $1/|S^2| \int_{S^2} \mathbf{T} \otimes \mathbf{T} |d\mathbf{T}| = \frac{1}{3} \mathbf{G}^{-1}$ together with (40) allows to convert the second integral on the right hand side of (43) into

$$\frac{1}{|S^2|} \int_{S^2} \mathbf{T} \cdot \mathbf{P}^T \mathbf{g} \mathbf{P} \mathbf{T} |d\mathbf{T}| = \frac{1}{3} \mathbf{A} : \bar{\mathbf{C}}. \quad (45)$$

Finally one obtains, neglecting again the constant terms, the closed form expression for the viscous part of the isochoric free energy as

$$\bar{\psi}^v = \bar{\psi}^v(\bar{\mathbf{C}}, \mathbf{A}) = \frac{1}{2} \mu^v [(\mathbf{A} : \bar{\mathbf{C}} - 3) - \ln(\det \mathbf{A})] \quad (46)$$

a neo-Hookean type expression independent of the influence of possible rotations of the microstructure based on the chosen form in (40). Consult again Remark 3 for a comparison of the resulting model with already existing models in the literature.

The resulting closed form expression for the viscous part of the isochoric free energy in (46) allows finally for the computation of a closed form expression for the corresponding viscous overstress based on (7) as

$$\bar{\tau}^v = \bar{\mathbf{F}} (2 \partial_{\bar{\mathbf{C}}} \bar{\psi}^v(\bar{\mathbf{C}}, \mathbf{A})) \bar{\mathbf{F}}^T = \mu^v \bar{\mathbf{F}} \mathbf{A} \bar{\mathbf{F}}^T. \quad (47)$$

Remark 3.

- Interestingly, the proposed model for the representation of the transient network to describe the rate-dependence yields the same expressions for the viscous part of the isochoric macroscopic free energy in (46) as well as for the corresponding viscous overstress in (47) as in Green and Tobolsky (1946). The transient changes in the network in Green and Tobolsky (1946) are explained by breakage and re-creation mechanisms with their rates being the main phenomenological quantities. Contrary, the current work introduces effective viscous mechanisms, representing the temporal chain interactions, through a phenomenological viscosity η . Based on the resulting identical expressions for the free energy and the overstresses, the same limitations do apply for both models.
- In the application of the transient model of Green and Tobolsky (1946) in Lubliner (1985) it is assumed that the determinant of the internal variable in (40) is constrained to be $\det \mathbf{A} = 1$ so that the last term in the expression of the isochoric part of the free energy in (46) cancels. In this work, $\det \mathbf{A} = 1$ in the initial state as well as after obtaining a fully relaxed state, but it may deviate from that value for states in between. Still, as outlined below, thermodynamic consistency of the formulation can be shown.

To outline the thermodynamic consistency of the proposed model one could easily refer to the starting point of the model in the form of the Smoluchowski equation which is shown to be dissipative in Remark 1. To assure that all the transformations performed in this section do not yield a different result, the proof is illustrated in detail.

Since the introduced internal variable \mathbf{A} in (40) is independent of the macrodeformation, the reduced dissipation inequality follows from (8) as

$$\mathcal{D}_{loc} = -2 \partial_{\mathbf{A}} \bar{\psi}^v : \frac{1}{2} \dot{\mathbf{A}} \geq 0 \quad (48)$$

with the satisfaction of the inequality to be shown in the following. Based on (46), the first term in (48) follows simply as $2 \partial_{\mathbf{A}} \bar{\psi}^v = \mu^v (\bar{\mathbf{C}} - \mathbf{A}^{-1})$ so that together with the evolution equation in (41) the dissipation can be expressed as

$$\mathcal{D}_{loc} = -\frac{\mu^v}{2\tau} (\bar{\mathbf{C}} - \mathbf{A}^{-1}) : (\bar{\mathbf{C}}^{-1} - \mathbf{A}) \geq 0 \quad (49)$$

where the inequality follows from the result of Theorem 1.

Theorem 1. Let $\bar{\mathbf{C}}$ be the isochoric part of the right Cauchy Green tensor and \mathbf{A} the symmetric tensorial internal variable of the developed diffusion-based micromechanical polymer model. Then the following inequality holds

$$(\bar{\mathbf{C}} - \mathbf{A}^{-1}) : (\bar{\mathbf{C}}^{-1} - \mathbf{A}) \leq 0. \quad (50)$$

Proof. Consider a polar decomposition of the two symmetric tensors $\bar{\mathbf{C}}$ and \mathbf{A} as well as their inverses in the form

$$\bar{\mathbf{C}} = \sum_{i=1}^{n_{dim}} \lambda_i \mathbf{u}_i \otimes \hat{\mathbf{u}}_i, \quad \mathbf{A} = \sum_{j=1}^{n_{dim}} \mu_j \mathbf{v}_j \otimes \hat{\mathbf{v}}_j \quad \text{and} \quad \bar{\mathbf{C}}^{-1} = \sum_{i=1}^{n_{dim}} \lambda_i^{-1} \hat{\mathbf{u}}_i \otimes \mathbf{u}_i, \quad \mathbf{A}^{-1} = \sum_{j=1}^{n_{dim}} \mu_j^{-1} \hat{\mathbf{v}}_j \otimes \mathbf{v}_j \quad (51)$$

where $\lambda_i > 0$, $\mu_j > 0$ are the positive eigenvalues and $\{\mathbf{u}_i, \tilde{\mathbf{u}}_i\}$, $\{\mathbf{v}_i, \tilde{\mathbf{v}}_i\}$ are the orthogonal eigenvectors of $\bar{\mathbf{C}}$ and \mathbf{A} , respectively. Since $\sum_i \mathbf{u}_i \otimes \tilde{\mathbf{u}}_i = \sum_j \mathbf{v}_j \otimes \tilde{\mathbf{v}}_j = \mathbf{1}$ and $\mathbf{1} : \mathbf{1} = 3$ the left hand side of (50) becomes

$$(\bar{\mathbf{C}} - \mathbf{A}^{-1}) : (\bar{\mathbf{C}}^{-1} - \mathbf{A}) = 6 - \sum_{ij} [\lambda_i \mu_j + \lambda_i^{-1} \mu_j^{-1}] (\mathbf{u}_i \otimes \tilde{\mathbf{u}}_i) : (\mathbf{v}_j \otimes \tilde{\mathbf{v}}_j). \quad (52)$$

To establish the inequality in (50), use is made of the identities $\alpha + \alpha^{-1} \geq 2$ for $\alpha > 0$ so that $\lambda_i \mu_j + \lambda_i^{-1} \mu_j^{-1} \geq 2$ and $(\mathbf{u}_i \otimes \tilde{\mathbf{u}}_i) : (\mathbf{v}_j \otimes \tilde{\mathbf{v}}_j) = (\mathbf{u}_i \cdot \mathbf{v}_j)(\tilde{\mathbf{u}}_i \cdot \tilde{\mathbf{v}}_j) = (\mathbf{u}_i \cdot \mathbf{v}_j)^2 \geq 0$ and finally

$$(\bar{\mathbf{C}} - \mathbf{A}^{-1}) : (\bar{\mathbf{C}}^{-1} - \mathbf{A}) \leq 6 - 2 \cdot \mathbf{1} : \mathbf{1} = 0 \quad (53)$$

showing (50). \square

4.3. Algorithmic representation and implementation

The algorithmic setting and implementation of the proposed model for the representation of the mobile viscous subnetworks within a time incremental formulation is briefly discussed in this section.

To do so, the evolution equation (41) of the symmetric tensorial internal variable \mathbf{A} needs to be discretized in time to advance from a given discrete time t_n towards $t_{n+1} = t_n + \Delta t$ within a single time step Δt . Application of an unconditional stable implicit backward Euler integration of (41) results in the update of the internal variable \mathbf{A} of a single viscous subnetwork as

$$\mathbf{A}_{n+1} = \frac{1}{1 + \Delta t / \tau} \left[\mathbf{A}_n + \frac{\Delta t}{\tau} \bar{\mathbf{C}}_{n+1}^{-1} \right] \quad (54)$$

in terms of the relaxation time $\tau = 1/6D^2$ with D^2 given in terms of solely microscopic objects in (26). Due to the linearity of the evolution equation (41), its algorithmic update in (54) is obtained in closed form. With the updated internal variable evaluated, the viscous overstress contribution follows from (47) as

$$\bar{\tau}_{n+1}^\nu = \mu^\nu \bar{\mathbf{F}}_{n+1} \mathbf{A}_{n+1} \bar{\mathbf{F}}_{n+1}^T = \mu^\nu \frac{1}{1 + \Delta t / \tau} \left[\bar{\mathbf{F}}_{n+1} \mathbf{A}_n \bar{\mathbf{F}}_{n+1}^T + \frac{\Delta t}{\tau} \mathbf{g}_{n+1}^{-1} \right] \quad (55)$$

in terms of the overstress moduli $\mu^\nu = nk_B \theta$. Finally, the sensitivity of the overstress update (55) to the variations of the deformation at time instance t_{n+1} yield the algorithmic tangent moduli in the form

$$\bar{\mathbf{C}}_{n+1}^\nu = 2 \partial_{\mathbf{g}} \bar{\tau}_{n+1}^\nu = -2 \mu^\nu \frac{\Delta t / \tau}{1 + \Delta t / \tau} \mathbb{I}_{\mathbf{g}^{-1}} \quad (56)$$

where $\mathbb{I}_{\mathbf{g}^{-1}}^{abcd} = [(\mathbf{g}^{-1})^{ac}(\mathbf{g}^{-1})^{bd} + (\mathbf{g}^{-1})^{ad}(\mathbf{g}^{-1})^{bc}] / 2$ is the fourth-order identity tensor written in terms of the inverse metric \mathbf{g}^{-1} .

Remark 4.

- It is emphasized that the result in (55) has to be combined with the elastic response coming from a chosen model for the elastic ground network in the way outlined in (7). The resulting isochoric response then further has to be combined with the spherical part as shown in (4) to obtain the final form of the stresses. In an analogous way the sensitivity of the final stresses is obtained where the expression in (56) results only from the sensitivity of the viscous overstress in (55) with regard to variations in the deformation.
- The results in (54)–(56) hold for a single viscous subnetwork in terms of microscopically motivated parameters τ and μ^ν . The proposed viscous model though consists of s viscous subnetworks resulting in totally $2s$ parameters. In particular, the s different relaxation times $\{\tau_i\}_{i=1}^s$ represent the broad dissipation spectra of the model, whereas the s viscous overstress moduli $\{\mu_i^\nu\}_{i=1}^s$ allow for different overstress stiffnesses of the model. Finally, the history of each of the branches is described by a separate internal variable \mathbf{A}_i resulting in the required storage of in total $6s$ scalar variables due to the symmetry of \mathbf{A} .

5. Representative numerical simulations

This section evaluates the capacity of the proposed diffusion-based viscoelasticity model by a comparison of the obtained numerical results with in the literature available experimental data sets. The essential requirement of the model is its ability to capture the specific viscoelastic response for different test scenarios of rubber-like materials at varying finite strains within a broad range of applied loading velocities. The material used throughout this section is a highly saturated nitrile butadiene rubber HNBR50 for which in Section 5.1 the parameters of the numerical model are fitted based on homogeneous uniaxial cyclic tests for an applied stretch λ_1 within the interval $\lambda_1 \in [0.75, 2.0]$. Section 5.2 then evaluates the model by simulating a similar uniaxial cyclic test but for an applied stretch within the purely compressive interval

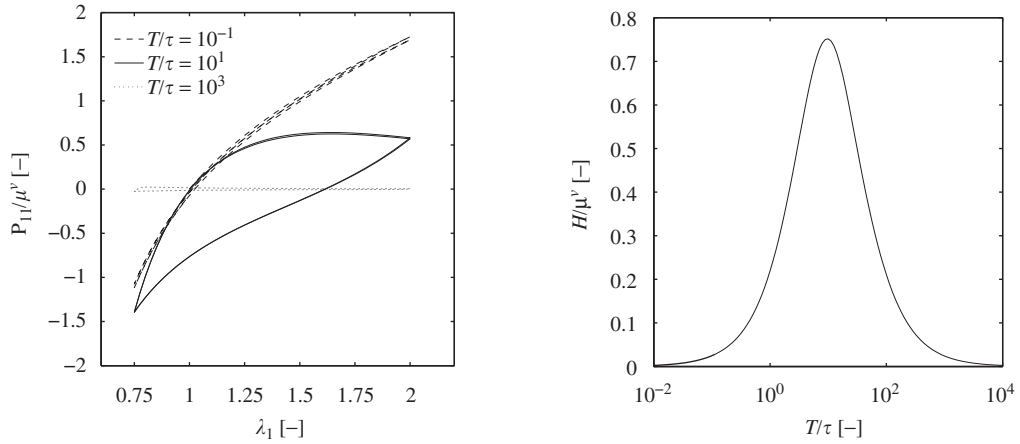


Fig. 7. Parameter fitting procedure. The illustration outlines the viscous response produced by a single branch. The relative overstress P_{11}/μ^v for loading periods T much lesser, comparable, and much greater than the relaxation time τ is shown on the left. The dependence of the relative hysteresis area H/μ^v of the first cycle on the ratio T/τ between the loading time and the relaxation time is shown on the right.

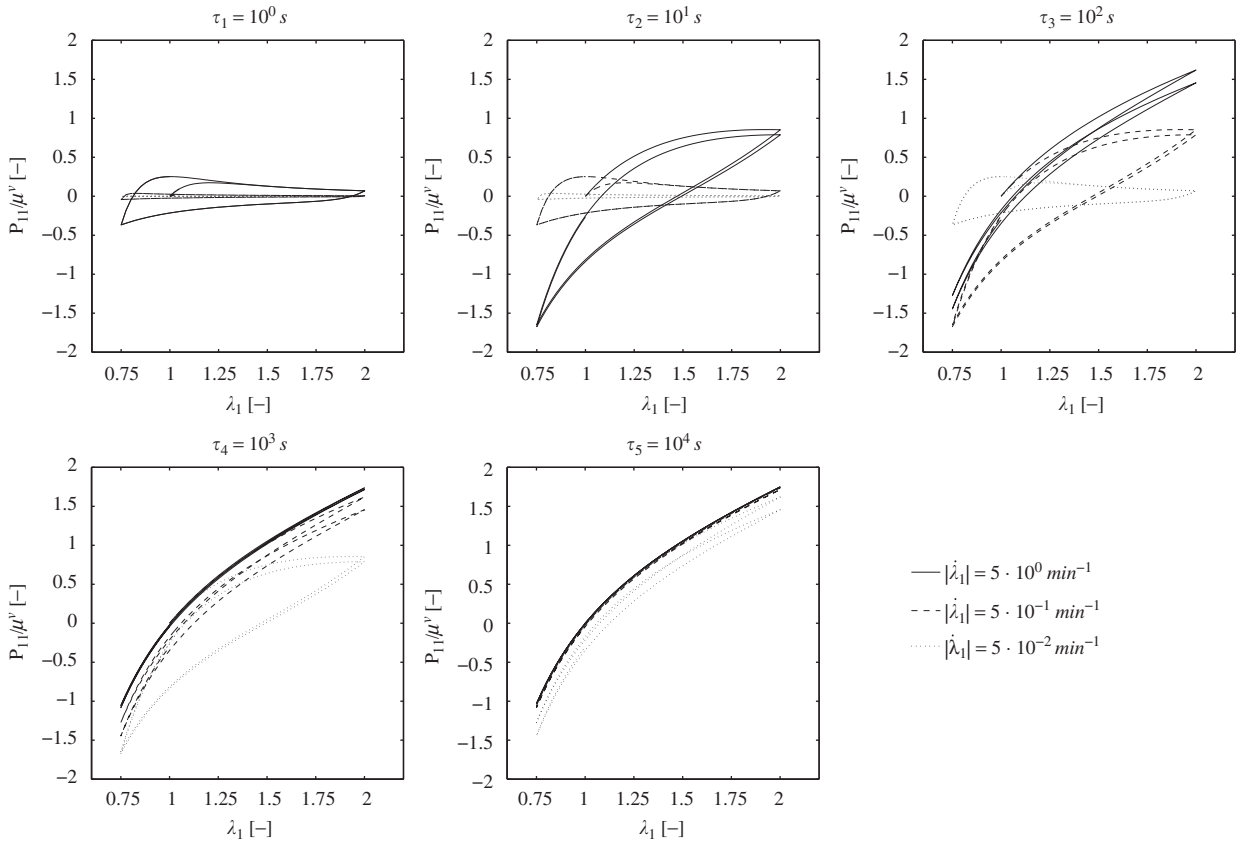


Fig. 8. Parameter fitting procedure. The illustration outlines the normalized overstress profiles for the $s=5$ viscous branches with the relaxation times $\{\tau_i\}_{i=1}^5 = \{10^0, 10^1, 10^2, 10^3, 10^4\}$ s and unit overstress moduli $\{\hat{\mu}_i^v\}_{i=1}^5 = 1$ MPa for the three considered uniaxial cyclic tests with different loading rates $|\dot{\lambda}_1| = 5 \times 10^0 \text{ min}^{-1}$, $|\dot{\lambda}_1| = 5 \times 10^{-1} \text{ min}^{-1}$, and $|\dot{\lambda}_1| = 5 \times 10^{-2} \text{ min}^{-1}$.

$\lambda_1 \in [0.75, 1.0]$ as well as for an applied stretch within the interval $\lambda_1 \in [0.75, 2.0]$ including several relaxation breaks. Finally, a non-homogeneous three-dimensional shear test is simulated in Section 5.3 for different loading conditions and compared with available experimental results.

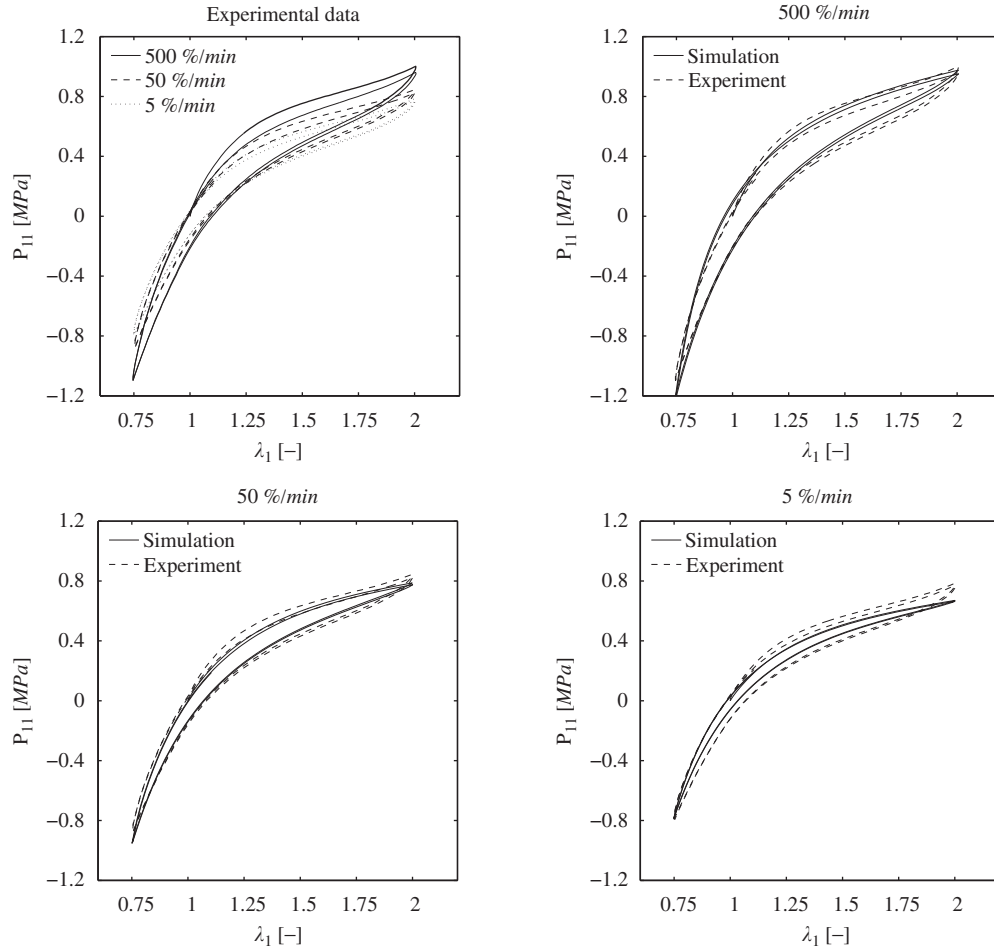


Fig. 9. Parameter fitting procedure. The illustration outlines a comparison of experimental results with the numerical results of the homogeneous uniaxial cyclic test for stretch values $\lambda_1 \in [0.75, 2.0]$. The upper left figure compares solely the experimental results (Miehe and Göktepe, 2005) for three different loading rates. The remaining illustrations compare these experimental results with the numerical obtained results for $|\dot{\lambda}_1| = 5 \times 10^0 \text{ min}^{-1}$ in the top right figure, for $|\dot{\lambda}_1| = 5 \times 10^{-1} \text{ min}^{-1}$ in the bottom left figure, and for $|\dot{\lambda}_1| = 5 \times 10^{-2} \text{ min}^{-1}$ in the bottom right figure using $\{\tau_i\}_{i=1}^5 = \{10^0, 10^1, 10^2, 10^3, 10^4\} \text{ s}$ for the relaxation time spectra and $\{\mu_i^v\}_{i=1}^5 = \{0.5357, 0.0762, 0.1205, 0.0213, 0.0229\} \text{ MPa}$ for the viscous overstress moduli.

5.1. Parameter fitting procedure

The experimental data set for this problem is taken from Miehe and Göktepe (2005) for a set of homogeneous uniaxial cyclic tests of a highly saturated nitrile butadiene rubber HNBR50 produced by the Robert Bosch GmbH. It is outlined in detail in Miehe and Göktepe (2005) that this material does not exhibit an equilibrium hysteresis so that its response can be considered as purely viscoelastic. In the following, the characteristic parameters of the model are fitted based on a homogeneous uniaxial cyclic test for an applied stretch λ_1 within the interval $\lambda_1 \in [0.75, 2.0]$. Based on the decomposition of the polymer microstructure into an elastic ground network and a viscous subnetwork, the corresponding parameters of the models representing both need to be fitted to the actual experimental results.

It is mentioned in Section 2 that the developed diffusion-based viscoelastic polymer model does not rely on the choice of a particular model for the representation of the elastic ground network. Therefore, throughout Section 5 the non-affine network model of Miehe et al. (2004) is chosen for the representation of the elastic response of the rubber-like material which is capable to produce an excellent fit when compared to the equilibrium response of HNBR50 for the homogeneous uniaxial experiments as outlined in Miehe and Göktepe (2005). In particular, in this work parameters close to those used in Miehe and Göktepe (2005) are obtained following the parameter fitting procedure outline in their work. The corresponding values are given as $N=5.2207$, $\mu=0.1602 \text{ MPa}$, $p=1.0666$, $U=11.2122$, and $q=0.2013$, representing the number of chain segments in the elastic ground network, the ground state stiffness, the non-affine stretch parameter, the tube geometry parameter, and the non-affine tube parameter, respectively, for the homogeneous uniaxial cyclic test outlined below.

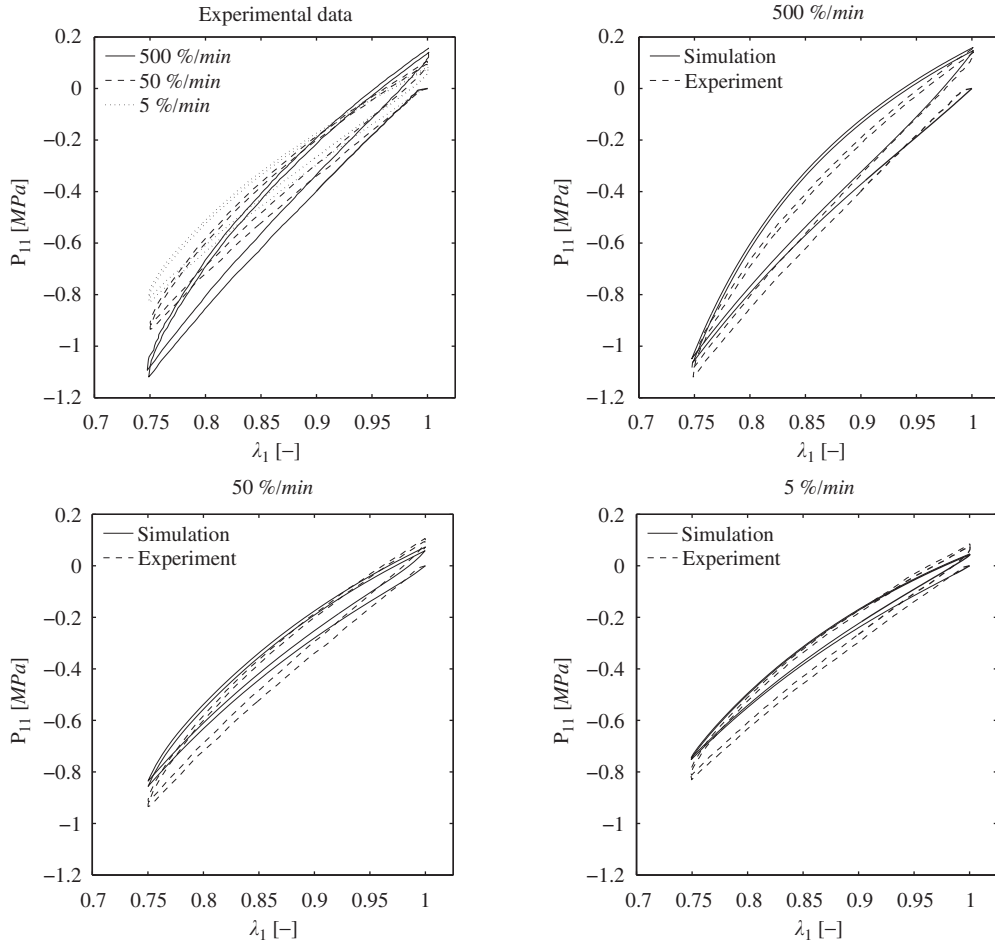


Fig. 10. Model verification through uniaxial cyclic tests. Comparison of experimental results with the numerical results for compressive stretch values $\lambda_1 \in [0.75, 1.0]$. The upper left figure compares solely the experimental results (Miehe and Göktepe, 2005) for three different loading rates. The remaining illustrations compare these experimental results with the numerical obtained results for $|\dot{\lambda}_1| = 5 \times 10^0 \text{ min}^{-1}$ in the top right figure, for $|\dot{\lambda}_1| = 5 \times 10^{-1} \text{ min}^{-1}$ in the bottom left figure, and for $|\dot{\lambda}_1| = 5 \times 10^{-2} \text{ min}^{-1}$ in the bottom right figure using $\{\tau_i\}_{i=1}^5 = \{10^0, 10^1, 10^2, 10^3, 10^4\} \text{ s}$ for the relaxation time spectra and $\{\mu_i^v\}_{i=1}^5 = \{0.5357, 0.0762, 0.1205, 0.0213, 0.0229\} \text{ MPa}$ for the viscous overstress moduli.

To fit the parameters for the developed viscoelastic part, a homogeneous uniaxial cyclic test performed at three different absolute loading rates $|\dot{\lambda}_1| = 5 \times 10^{-2} \text{ min}^{-1}$, $|\dot{\lambda}_1| = 5 \times 10^{-1} \text{ min}^{-1}$, and $|\dot{\lambda}_1| = 5 \times 10^0 \text{ min}^{-1}$ of that same material is used. It is emphasized that the actual loading rates might deviate from these values due to a decreasing accuracy of the experimental measurements especially for low loading rates. The stretch region of the specimen is assumed to fall within the closed interval $\lambda_1 \in [0.75, 2.0]$. The experimental stress-stretch curves in terms of the P_{11} component of the First Piola Kirchhoff stress tensor $\mathbf{P} = \tau \mathbf{F}^{-T}$ are depicted in the upper left illustration of Fig. 9. One observes a characteristic response for viscoelastic materials in the form of a stiffer behavior for an increasing loading rate. Also the area of the resulting hysteresis curves, representing the amount of dissipated energy per cycle, gets larger as the loading rate increases from $5 \times 10^{-2} \text{ min}^{-1}$ to $5 \times 10^0 \text{ min}^{-1}$. Finally, one can observe the difference between the first and second cycles of the loading being more distinct for higher loading velocities. In particular one should notice the change of the viscoelastic modulus after the first cycle of loading.

To determine whether the proposed model is capable of capturing such an experimentally observed viscoelastic response a parametric analysis is performed. A single viscous subnetwork responsible for the resulting viscous overstress is considered in terms of the two parameters in the form of the viscous overstress modulus μ^v and the relaxation time τ . Whereas the former trivially scales the amount of the overstress, the latter has a more peculiar impact which can be illustrated for the cyclic uniaxial test considered here. In particular, the left illustration of Fig. 7 shows the overstress produced by the considered viscous branch depending on the period of the altering stretch $T = 2(\lambda_1^{\max} - \lambda_1^{\min})/|\dot{\lambda}_1|$. One can observe that the response differs from the stiff quasi-elastic one for $T/\tau \ll 1$ corresponding to a very quick loading to an almost vanishing one for $T/\tau \gg 1$ corresponding to an extremely slow loading. In the first case there is no time for any changes to occur in the viscous subnetwork during the loading period, whereas in the latter case the loading is so slow that

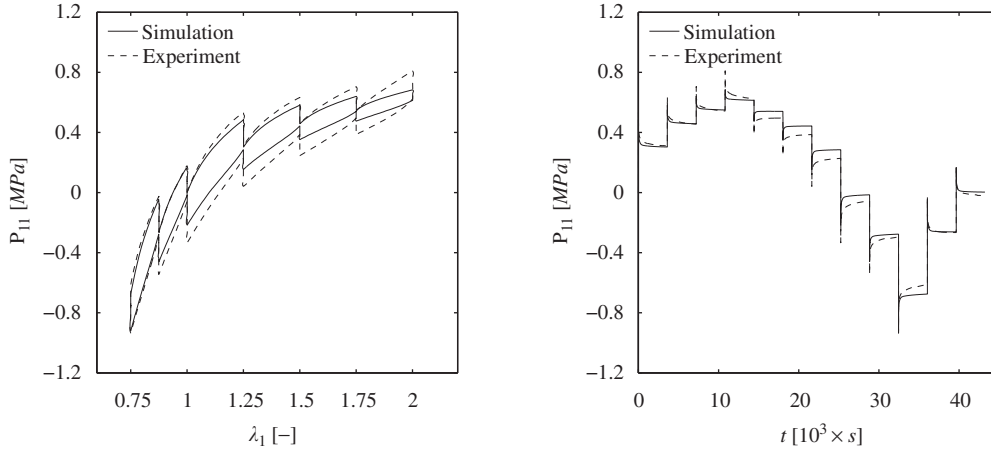


Fig. 11. Model verification through uniaxial cyclic tests. Comparison of experimental results (Miehe and Göktepe, 2005) with the numerical results for stretch values $\lambda_1 \in [0.75, 2.0]$ including relaxation breaks at stretch values $\lambda_1 = 0.75, 0.875, 1.0, 1.25, 1.5, 1.75, 2.0$. The strain–stress diagram comparison is shown on the left whereas the stress–time relation is shown on the right using $\{\tau_i\}_{i=1}^s = \{10^0, 10^1, 10^2, 10^3, 10^4\}$ s for the relaxation time spectra and $\{\mu_i^v\}_{i=1}^s = \{0.5357, 0.0762, 0.1205, 0.0213, 0.0229\}$ MPa for the viscous overstress moduli.

the subnetwork has more than sufficient time to relax fully to an unperturbed stress-free configuration. The viscous hysteresis is only observed at loading rates for which the stretch period T is comparable to the relaxation time τ . This fact is illustrated by the diagram on the right of Fig. 7 depicting the dependence of the amount of the energy dissipated during the first cycle on the ratio T/τ . This curve shows that a single viscous branch with a given relaxation time will produce any viscous hysteresis only within a certain range of loading velocities. Its span can be limited to a change of magnitude of approximately 2 orders of the T/τ ratio.

For the representation of the real relaxation spectrum several viscous branches need to be considered. In particular, to fit the parameters of the experimental stress–stretch curves in the upper left illustration of Fig. 9, a discrete spectrum of $s=5$ relaxation times $\{\tau_i\}_{i=1}^s = \{10^0, 10^1, 10^2, 10^3, 10^4\}$ s is chosen. With the elastic part of the deviatoric stresses obtained through the non-affine network model in Miehe et al. (2004), the only remaining parameters to be identified are the corresponding overstress moduli $\{\mu_i^v\}_{i=1}^s$. Their values are determined by a simple procedure exploiting the linear dependence of the total overstress on the viscous moduli. To do so, the deviatoric part of the stresses is computed based on (7) as

$$\bar{\tau}(t) = \bar{\tau}^e(t) + \sum_{i=1}^s \bar{\tau}_i^v(t) \quad (57)$$

in terms of the elastic equilibrium stress $\bar{\tau}^e$ and the viscous overstresses $\{\bar{\tau}_i^v\}_{i=1}^s$. Denoting the cyclic tests in Fig. 9 by the indices a, b , and c for the different loading rates, one can compute the stress as a mere combination

$$\bar{\tau}^{abc}(t) = \bar{\tau}^{e,abc}(t) + \sum_{i=1}^s \mu_i^v \bar{\tau}_i^{v,abc}(t) \quad (58)$$

where $\{\bar{\tau}_i^{v,abc}\}_{i=1}^s$ are the normalized overstress profiles shown in Fig. 8 that can be computed separately for each of the s branches with a unit moduli assigned as $\{\bar{\mu}_i^v\}_{i=1}^s = 1$ MPa and the loading rates corresponding to the tests a, b , and c . The overstress moduli $\{\mu_i^v\}_{i=1}^s$ are then obtained by minimizing the discrepancy of the stress–strain curves computed by (58) to the experimental ones illustrated in the upper left illustration of Fig. 9.

Overstress moduli $\{\mu_i^v\}_{i=1}^s = \{0.5357, 0.0762, 0.1205, 0.0213, 0.0229\}$ MPa are finally obtained as the result of this procedure. The obtained fit for the cyclic uniaxial tension–compression tests is depicted in the illustrations of Fig. 9 for the different applied loading rates. The experimental features of the true viscoelastic response are captured reasonably well by this fit. The level of the stresses and the thickness of the individual hysteresis curves achieved at the three different loading rates comply rather well with the experimental data. Some discrepancy can be observed when looking at the difference between the first and the second cycles of the loading which is predicted smaller by the simulations when compared to the actual experimental results.

5.2. Model verification through uniaxial cyclic tests

After having obtained the characteristic model parameters through the fitting procedure described above in Section 5.1, the model with those material parameters is used to simulate two further tests, different from the

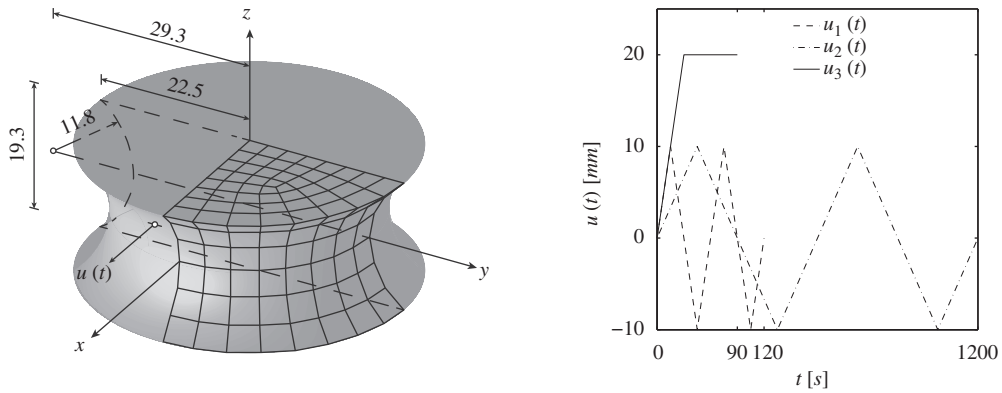


Fig. 12. Model verification through non-homogeneous 3D shear tests. The geometry of the rubber specimen with dimensions in *mm* together with the finite element discretization of one quarter of the specimen is shown on the left. The boundary conditions are such that the bottom surface is fully restrained and the whole top surface is displaced by $u(t)$ in x -direction. The individual loading conditions are shown on the right in the form of two cyclic loadings $u_1(t)$ and $u_2(t)$ for different loading rates $|\dot{u}_1| = 40$ mm/min and $|\dot{u}_2| = 4$ mm/min and in the form of a relaxation loading $u_3(t)$ where u_3 is held constant for 60 s after reaching $u_3 = 20$ mm in 30 s.

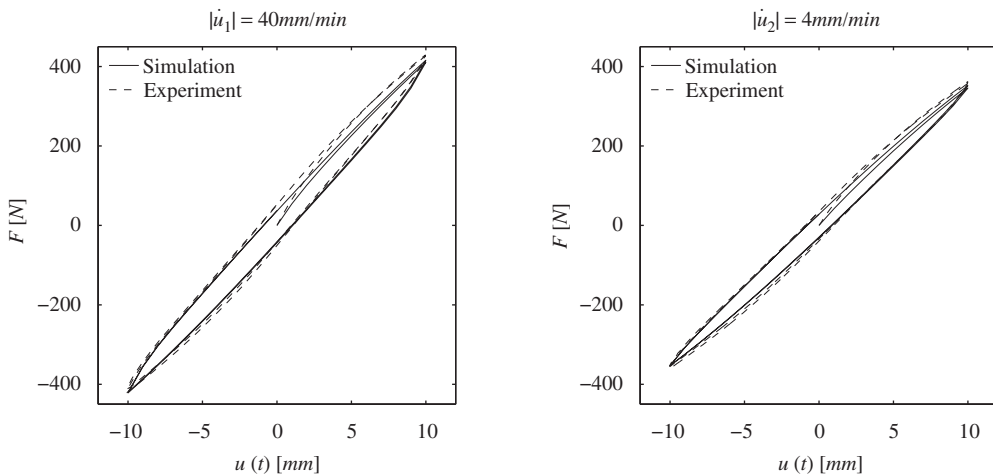


Fig. 13. Model verification through non-homogeneous 3D shear tests. Illustration of the load-deflection diagrams obtained for the cyclic loading conditions and comparison with the experimental results from Miehe and Göktepe (2005) for $|\dot{u}_1| = 40$ mm/min on the left and $|\dot{u}_2| = 4$ mm/min on the right. A good agreement of the attained extremal force values and the shape of the hysteresis can be observed.

one above. A comparison with available experimental results will then allow for an evaluation of the quality of the model.

The first example is a purely compressive uniaxial tests performed for the same HNBR50 material (Miehe and Göktepe, 2005). The considered stretch values fall within the compressive interval $\lambda_1 \in [0.75, 1.0]$ at three different loading rates $|\dot{\lambda}_1| = 5 \times 10^{-2} \text{ min}^{-1}$, $5 \times 10^{-1} \text{ min}^{-1}$ and $5 \times 10^0 \text{ min}^{-1}$. The above mentioned features of the viscoelastic response at cyclic loading such as the rate-dependent stiffening, hysteresis growth and difference of the first cycle to the subsequent ones are captured also for this test as it is illustrated in Fig. 10. However, the experimental data outlined in the top left illustration of Fig. 10 are not fully reproduced by the simulation. Particularly, it can be seen that the viscoelastic moduli are underestimated so that substantially a softer response is predicted by the model with the parameter fit obtained above. The fitting illustrated in Fig. 9 captures nicely only the value of the tangent modulus on the second cycle of the loading, whereas its value in the beginning of the loading, which coincides for the compressive and tensile dominated tests, remains underestimated.

The second example to verify the quality of the developed model studies a homogeneous experiment on HNBR50 (Miehe and Göktepe, 2005) which captures the relaxation during breaks in tension-compression cyclic tests. The same specimen as in the preceding tests is subsequently loaded and unloaded in a stepwise manner. At each step the stretch changes from one intermediate value to the next one with an absolute loading rate of $|\dot{\lambda}_1| = 3 \times 10^0 \text{ min}^{-1}$ which is kept at a constant deformation thereafter for a one-hour period. The hold stretch values are $\lambda_1 = 0.75, 0.875, 1.0, 1.25, 1.5, 1.75,$ and 2.0 . Altogether the experiment involves 12 relaxation tests, which allow to observe the overstress development at different

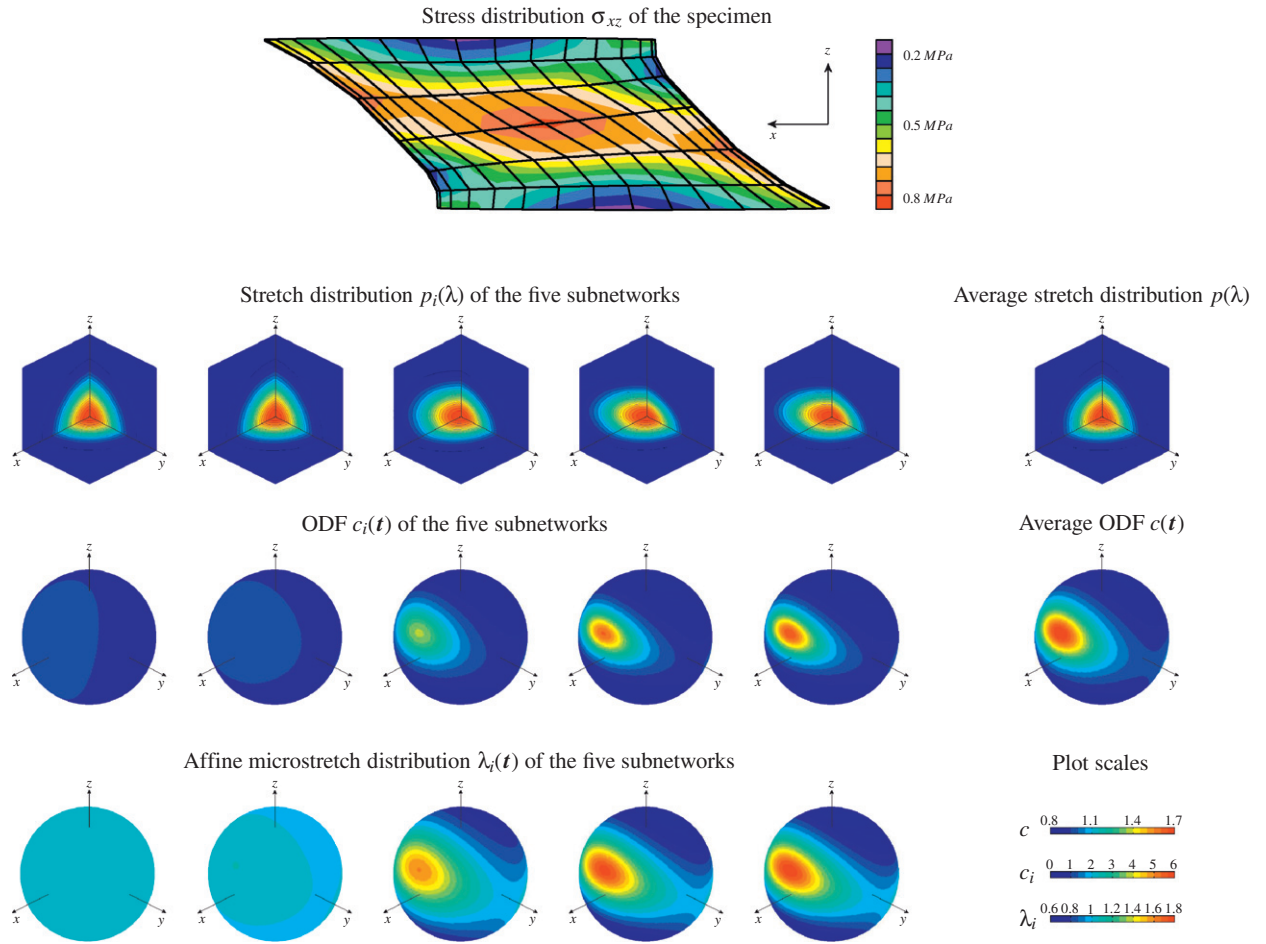


Fig. 14. Model verification through non-homogeneous 3D shear tests. At the top, an illustration of the obtained stress distribution σ_{xz} of the specimen for the third loading condition at the beginning of the relaxation process at time $t=30$ s is shown. Below follow illustrations of the internal state of the material point placed in the geometric center of the specimen based on the stretch distribution $p_i(\lambda)$, the orientation density function (ODF) $c_i(t)$, and the affine microstretch distribution $\lambda_i(t)$ of the five subnetworks for the chosen relaxation times $\{\tau_i\}_{i=1}^5 = \{10^0, 10^1, 10^2, 10^3, 10^4\}$ s. In addition the average stretch distribution $p(\lambda)$ and the average ODF $c(t)$ are shown.

stretch levels as well as its relaxation in detail. When comparing the numerical and experimental results based on the illustration in Fig. 11, one observes that the fit is quite good in the compressive part of the test and at the moderate tensile stretches up to the second break. In particular, the relaxation of the viscoelastic stress during the breaks is captured well in time. To the contrary, at higher tensile stretches the development of the overstress does not match the experimental data. According to the proposed model, the evolution of the overstress is linearly proportional to the deformation velocity \mathbf{l} (in particular to its component $l_{11} = \dot{\lambda}_1/\lambda_1$ in the case of the uniaxial loading), which for the given stretch velocity $|\dot{\lambda}_1|$ gets smaller at higher stretches. Correspondingly, the overstress values and the thickness of the hysteresis between the second and the sixth break get lower as the stretch increases.

5.3. Model verification through non-homogeneous three-dimensional shear tests

Next, the proposed model is evaluated based on its performance when solving a three-dimensional (3D) problem. The numerical implementation follows the discussion outlined in Section 4.3. Considered is a non-homogeneous shear experiment in 3D. The specimen is a body of revolution with a concave toroidal lateral surface. Its geometry and dimensions are illustrated on the left of Fig. 12. The boundary conditions are such that during the experiment the whole bottom face of the specimen is fixed, whereas the whole top face is subjected to a horizontal displacement in x -direction. The material of the rubber block, for which experimental results are available from Miede and Göktepe (2005), is the one used before in the form of a highly saturated nitrile butadiene rubber HNR50. The elastic and viscous parameters needed for the numerical simulation are the ones obtained through the parameter fitting procedure in Section 5.1.

Three loading functions $\{u_i(t)\}_{i=1}^3$ for the horizontal displacement are considered of which two correspond to cyclic deformations for $u \in [-10, 10]$ mm at two different loading velocities $|\dot{u}_1| = 40$ mm/min and $|\dot{u}_2| = 4$ mm/min. The third

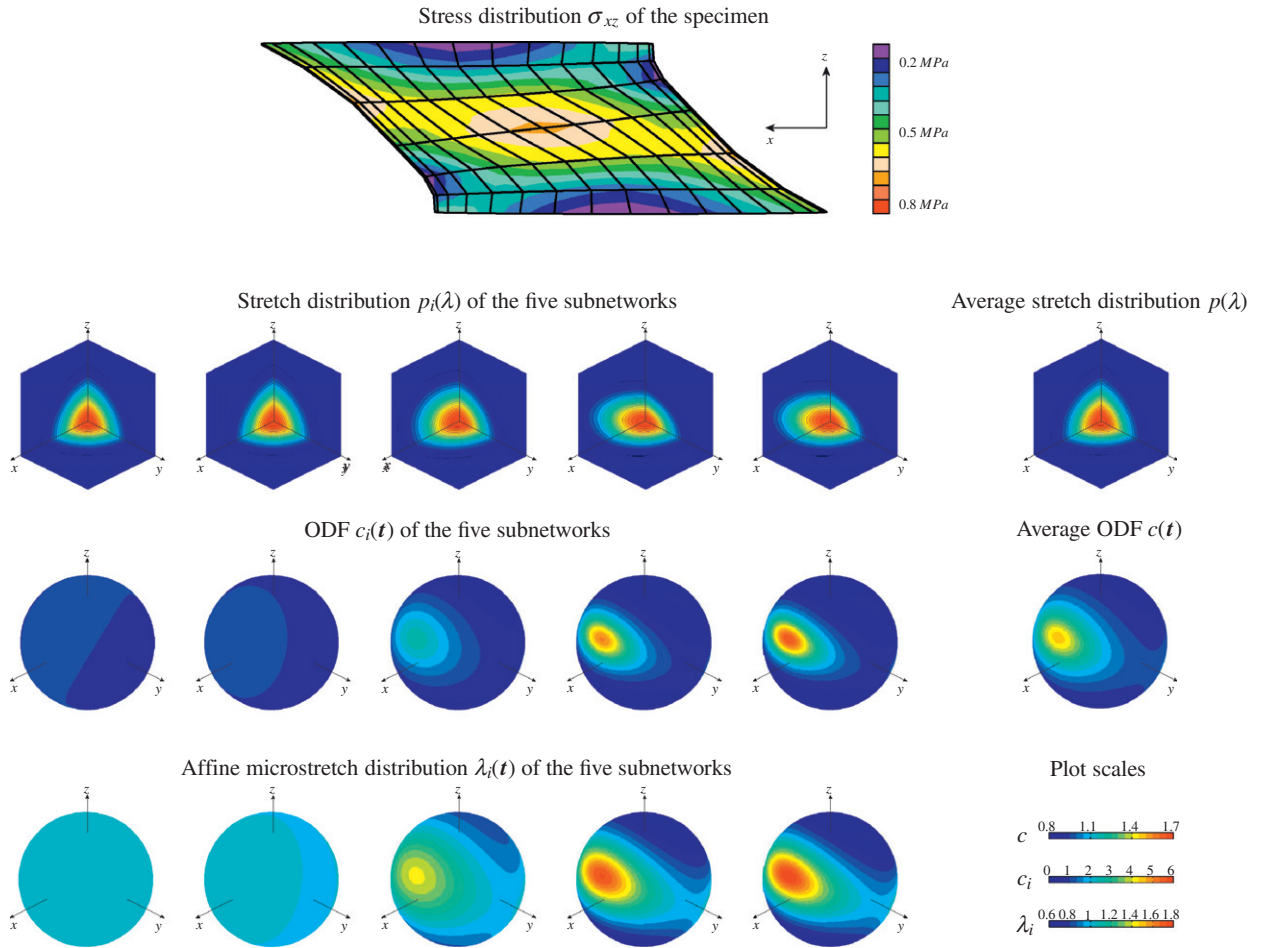


Fig. 15. Model verification through non-homogeneous 3D shear tests. At the top, an illustration of the obtained stress distribution σ_{xz} of the specimen for the third loading condition at the end of the relaxation process at time $t=90$ s is shown. Below follow illustrations of the internal state of the material point placed in the geometric center of the specimen based on the stretch distribution $p_i(\lambda)$, the orientation density function (ODF) $c_i(\mathbf{t})$, and the affine microstretch distribution $\lambda_i(\mathbf{t})$ of the five subnetworks for the chosen relaxation times $\{\tau_i\}_{i=1}^5 = \{10^0, 10^1, 10^2, 10^3, 10^4\}$ s. In addition the average stretch distribution $p(\lambda)$ and the average ODF $c(\mathbf{t})$ are shown.

loading represents a relaxation test at which the top surface is moved in 30 s at a constant rate $|\dot{u}_3| = 40$ mm/min up to a displacement of $u_3 = 20$ mm after which a relaxation period of 60 s follows. An illustration of the loading processes is given on the right of Fig. 12.

The obtained numerical results of this rubber specimen are simulated using 1152 eight-node Q1P0 mixed brick finite elements. A comparison with the experimental results for the two cyclic tests is shown in Fig. 13 in the form of the obtained load-deflection diagrams for the loading rate $|\dot{u}_1| = 40$ mm/min on the left and $|\dot{u}_2| = 4$ mm/min on the right of that illustration. The results show good agreement since the extremal force values attained in both tests as well as the shape of the viscous hysteresis do agree with quite good precision. Again, the initial response to the first loading (from $u=0$ to 10 mm) is reproduced not as good as the subsequent cycles.

The third loading scenario is evaluated in Figs. 14 and 15, showing the true shear stress contours at the end of the loading at time $t=30$ s and after the relaxation period at time $t=90$ s, respectively. One can observe quite a substantial relaxation of the stress depicted at the top of both figures in the form of the outlined σ_{xz} stress distribution. The perturbation induced by the initial deformation of the material decays due to the diffusion mechanisms discussed in Section 4. The extend to which the microdeformation relaxes is naturally different for the five mobile subnetworks. An important observation is, that the diffusional motion of the mobile chains results both, in re-orientation and stretch relaxation as further shown in Figs. 14 and 15. Observed is the evolution of the internal state of the material point placed in the geometric center of the specimen. This is given by the partial distributions of the stretch $p_i(\lambda) = P(\mathbf{P}_i^{-1}\lambda)/\det(\mathbf{P}_i)$ in the five mobile subnetworks. The average stretch distribution in the overall mobile network $p(\lambda) = 1/n \sum_{i=1}^5 n_i p_i(\lambda)$ represents the total re-distribution of the stretch vector. This re-distribution incorporates both re-orientation and stretch relaxation. The former is illustrated by the orientation density functions plotted over the

spatial directions \mathbf{t} in the orientation space and retrieved for each of the subnetworks as $c_i(\mathbf{t}) = 4\pi \int_0^\infty p(\lambda\mathbf{t})\lambda^2 d\lambda$ where the factor 4π comes from the convention that a homogeneous distribution corresponds to $c_i(\mathbf{t}) = 1$. The average for all the mobile polymer chains $c(\mathbf{t}) = 1/n \sum_{i=1}^5 n_i c_i(\mathbf{t})$ is shown on the right of that row. The stretch relaxation is presented by the distribution of the affine microstretch over the directions $\lambda_i(\mathbf{t}) = (\mathbf{P}_i^{-1}\mathbf{t} \cdot \mathbf{P}_i^{-1}\mathbf{t})^{-1/2}$ shown at the very bottom of Figs. 14 and 15.

6. Conclusion

A new micromechanically motivated transient network model is developed in this work and incorporated into the framework of finite rubber viscoelasticity. The model is based on diffusion processes of the highly mobile macromolecules forming the individual polymer chains. These processes result in the evolution of the probability for finding chain segments within a certain stretch state which is governed by the generalization of the Smoluchowski equation from non-interacting particles towards flexible polymer chains in this work. It is shown how a tensorial representation of such evolution yields closed form expressions of the viscous part of the isochoric free energy as well as for the viscous overstress which interestingly agree with the corresponding expressions obtained in the transient network theory of Green and Tobolsky (1946), even though the underlying micromechanical model differs. Finally, the model is evaluated based on its application in homogeneous and non-homogeneous tests where the numerical results are compared with in the literature available experimental data sets. In those simulations, the non-affine network model of Miehe et al. (2004) is chosen for the representation of the elastic response. The obtained results are satisfactory when taken into account the simplicity of the obtained viscous response in the proposed transient network model.

Modifications of the micromechanically motivated model in the sense that it results in more advanced evolution laws for the polymer stretch probability may be achieved by differently accounting for translational and rotational degrees of freedom on the microscopic level. It is furthermore desired to develop a microscopic model which yields a physical based discrete relaxation spectra. These are possible directions for future research in this area.

Acknowledgments

Financial support for this research was provided by the “Juniorprofessorenprogramm des Landes Baden-Württemberg” and the German Research Foundation (DFG) within the Cluster of Excellence in Simulation Technology (EXC 310/1) at the University of Stuttgart. This support is gratefully acknowledged.

References

- Arruda, E., Boyce, M., 1993a. A three-dimensional constitutive model for the large stretch behavior of rubber elastic materials. *J. Mech. Phys. Solids* 41, 389–412.
- Arruda, E., Boyce, M., 1993b. Evolution of plastic anisotropy in amorphous polymers during finite straining. *Int. J. Plast.* 9, 697–720.
- Bergström, J., Boyce, M., 1998. Constitutive modeling of the large strain time-dependent behavior of elastomers. *J. Mech. Phys. Solids* 46, 931–954.
- Bernstein, B., Kearsley, E., Zapas, L., 1963. A study of stress relaxation with finite strain. *J. Rheol.* 7, 391–410.
- Bird, R., Hassager, O., Armstrong, R., Curtiss, C., 1977. *Dynamics of Polymeric Liquids, Kinetic Theory*. Wiley, New York.
- Boyce, M., Arruda, E., 2000. Constitutive models of rubber elasticity: a review. *Rubber Chem. Technol.* 73, 716–725.
- Boyce, M., Parks, D., Argon, A., 1988. Large inelastic deformation of glassy polymers. Part 1: rate dependent constitutive model. *Mech. Mater.* 7, 15–33.
- Boyce, M., Parks, D., Argon, A., 1989. Plastic flow in oriented glassy polymers. *Int. J. Plast.* 5, 593–615.
- Cotten, G., Boonstra, B., 1965. Stress relaxation in rubbers containing reinforced fillers. *J. Appl. Polym. Sci.* 9, 3395–3408.
- De Gennes, P., 1971. Reptation of a polymer chain in the presence of fixed obstacles. *J. Chem. Phys.* 55, 572–579.
- Deam, R., Edwards, S., 1976. The theory of rubber elasticity. *Philos. Trans. R. Soc. London, Ser. A* 280, 317–353.
- Doi, M., Edwards, S., 1986. *The Theory of Polymer Dynamics*. Clarendon Press, Oxford.
- Edwards, S., 1967. The statistical mechanics of polymerized materials. *Proc. Phys. Soc.* 92, 9–16.
- Edwards, S., Vilgis, T., 1988. The tube model theory of rubber elasticity. *Rep. Prog. Phys.* 51, 243–297.
- Erman, B., Flory, P., 1978. Theory of elasticity of polymer networks. II. The effect of geometric constraints on junctions. *J. Chem. Phys.* 68, 5363–5369.
- Ferry, J., 1980. *Viscoelastic Properties of Polymers*. John Wiley and Sons, Inc.
- Flory, P., 1944. Network structure and the elastic properties of vulcanized rubber. *Chem. Rev.* 35, 51–75.
- Flory, P., 1953. *Principles of Polymer Chemistry*. Cornell University Press.
- Flory, P., 1977. Theory of elasticity of polymer networks. The effect of local constraints on junctions. *J. Chem. Phys.* 66, 5720–5729.
- Flory, P., Erman, B., 1982. Theory of elasticity of polymer networks. 3. *Macromolecules* 15, 800–806.
- Flory, P., Gordon, M., McCrum, N., 1976. Statistical thermodynamics of random networks. *Proc. R. Soc. London, Ser. A* 351, 351–380.
- Flory, P., Rehner Jr., J., 1943. Statistical mechanics of cross-linked polymer networks: I. Rubberlike elasticity. *J. Chem. Phys.* 11, 512–520.
- Göktepe, S., Miehe, C., 2008. Efficient two-scale modeling of finite rubber viscoelasticity. *Tech. Mech.* 28, 22–32.
- Govindjee, S., Reese, S., 1997. A presentation and comparison of two large deformation viscoelasticity models. *J. Eng. Mater. Technol.* 119, 251–255.
- Green, M., Tobolsky, A., 1946. A new approach to the theory of relaxing polymeric media. *J. Chem. Phys.* 14, 80–92.
- Guth, E., Mark, H., 1934. Zur innermolekularen Statistik, insbesondere bei Kettenmolekülen I. *Monatsh. Chem.* 65, 93–121.
- Heinrich, G., Kaliske, M., 1997. Theoretical and numerical formulation of a molecular based constitutive tube-model of rubber elasticity. *Comput. Theor. Polym. Sci.* 7, 227–241.
- Heinrich, G., Straube, E., 1983. On the strength and deformation dependence of the tube-like topological constraints of polymer networks, melts and concentrated solutions. I. The polymer network case. *Acta Polym.* 34, 589–594.
- Heinrich, G., Straube, E., 1984. On the strength and deformation dependence of the tube-like topological constraints of polymer networks, melts and concentrated solutions. II. Polymer melts and concentrated solutions. *Acta Polym.* 35, 115–119.
- Holzapfel, G., Simo, J., 1996. A new viscoelastic constitutive model for continuous media at finite thermomechanical changes. *Int. J. Solids Struct.* 33, 3019–3034.

- James, A., Green, A., 1975. Strain energy functions of rubber. II. The characterization of filled vulcanizates. *J. Appl. Polym. Sci.* 19, 2319–2330.
- James, A., Green, A., Simpson, G., 1975. Strain energy functions of rubber. I. Characterization of gum vulcanizates. *J. Appl. Polym. Sci.* 19, 2033–2058.
- James, H., Guth, E., 1943. Theory of elastic properties of rubber. *J. Chem. Phys.* 11, 455–481.
- Kaliske, M., Heinrich, G., 1999. An extended tube-model for rubber elasticity: statistical-mechanical theory and finite element implementation. *Rubber Chem. Technol.* 72, 602–632.
- Kaliske, M., Rothert, H., 1997. Formulation and implementation of three-dimensional viscoelasticity at small and finite strains. *Comput. Mech.* 19, 228–239.
- Kuhn, W., 1934. Über die Gestalt fadenförmiger Moleküle in Lösungen. *Colloid. Polym. Sci.* 68, 2–15.
- Kuhn, W., 1936. Beziehungen zwischen Molekülgröße, statistischer Molekülgestalt und elastischen Eigenschaften hochpolymerer Stoffe. *Colloid. Polym. Sci.* 76, 258–271.
- Kuhn, W., Grün, F., 1942. Beziehungen zwischen elastischen Konstanten und Dehnungsdoppelbrechung hochelastischer Stoffe. *Colloid. Polym. Sci.* 101, 248–271.
- Lee, E., 1969. Elastic-plastic deformation at finite strains. *J. Appl. Mech.* 36, 1–6.
- Lion, A., 1996. A constitutive model for carbon black filled rubber. Experimental investigations and mathematical representations. *Continuum. Mech. Thermodyn.* 8, 153–169.
- Lodge, A., 1956. A network theory of flow birefringence and stress in concentrated polymer solutions. *Trans. Faraday Soc.* 52, 120–130.
- Lubliner, J., 1985. A model of rubber viscoelasticity. *Mech. Res. Commun.* 12, 93–99.
- Marckmann, G., Verron, E., 2006. Comparison of hyperelastic models for rubberlike materials. *Rubber Chem. Technol.* 79, 835–858.
- Marsden, J., Hughes, T., 1983. *Mathematical Foundations of Elasticity*. Dover Publications, New York.
- Meyer, K., von Susich, G., Valkó, 1932. Die elastischen Eigenschaften der organischen Hochpolymeren und ihre kinetische Deutung. *Colloid. Polym. Sci.* 59, 208–216.
- Miehe, C., 1998. A constitutive frame of elastoplasticity at large strains based on the notion of a plastic metric. *Int. J. Solids Struct.* 35, 3859–3897.
- Miehe, C., Göktepe, S., 2005. A micro-macro approach to rubber-like materials. Part II: the micro-sphere model of finite rubber viscoelasticity. *J. Mech. Phys. Solids* 53, 2231–2258.
- Miehe, C., Göktepe, S., Lulei, F., 2004. A micro-macro approach to rubber-like materials—part I: the non-affine micro-sphere model of rubber elasticity. *J. Mech. Phys. Solids* 52, 2617–2660.
- Miehe, C., Keck, J., 2000. Superimposed finite elastic-viscoelastic-plastoelastic stress response with damage in filled rubbery polymers, experiments, modelling and algorithmic implementation. *J. Mech. Phys. Solids* 48, 323–365.
- Mooney, M., 1940. A theory of large elastic deformation. *J. Appl. Phys.* 11, 582–592.
- Ogden, R., 1972. Large deformation isotropic elasticity—on the correlation of theory and experiment for incompressible rubberlike solids. *Proc. R. Soc. London, Ser. A* 326, 565–584.
- Reese, S., Govindjee, S., 1998. A theory of finite viscoelasticity and numerical aspects. *Int. J. Solids Struct.* 35, 3455–3482.
- Reese, S., Wriggers, P., 1999. Modelling of the thermo-mechanical material behaviour of rubber-like polymers—Micromechanical motivation and numerical simulation. In: Dorfmann, A., Muhr, A. (Eds.), *Constitutive Models for Rubber*, pp. 13–21.
- Rivlin, R., 1948. Large elastic deformations of isotropic materials. I. Fundamental concepts II. Some uniqueness theorems for pure, homogeneous deformation. III. Some simple problems in cylindrical polar coordinates. *Philos. Trans. R. Soc. London, Ser. A* 240, 459–525.
- Rivlin, R., Saunders, D., 1951. Large elastic deformation of isotropic materials VII. Experiments on the deformation of rubber. *Philos. Trans. R. Soc. London, Ser. A* 243, 251–288.
- Ronca, G., Allegra, G., 1975. An approach to rubber elasticity with internal constraints. *J. Chem. Phys.* 63, 4990–4997.
- Sidoroff, F., 1974. Un modèle viscoélastique non linéaire avec configuration intermédiaire. *J. Méc.* 19, 2319–2330.
- Simo, J., 1987. On a fully three-dimensional finite-strain viscoelastic damage model: formulation and computational aspects. *Comput. Methods Appl. Mech. Eng.* 60, 153–173.
- Staudinger, H., 1920. Über Polymerisation. *Ber. Dtsch. Chem. Ges.* 53, 1073–1085.
- Sullivan, J., 1986. The relaxation and deformation properties of a carbon-black filled elastomer in biaxial tension. *J. Polym. Sci., Part B: Polym. Phys.* 24, 161–173.
- Tanaka, F., Edwards, S., 1992. Viscoelastic properties of physically cross-linked networks. Transient network theory. *Macromolecules* 25, 1516–1523.
- Treloar, L., 1943a. The elasticity of a network of long-chain molecules I. *Trans. Faraday Soc.* 39, 36–41.
- Treloar, L., 1943b. The elasticity of a network of long-chain molecules II. *Trans. Faraday Soc.* 39, 241–246.
- Treloar, L., 1944. Stress-strain data for vulcanised rubber under various types of deformation. *Trans. Faraday Soc.* 40, 59–70.
- Treloar, L., 1946. The elasticity of a network of long-chain molecules III. *Trans. Faraday Soc.* 42, 83–94.
- Treloar, L., 1954. The photoelastic properties of short-chain molecular networks. *Trans. Faraday Soc.* 50, 881–896.
- Treloar, L., 1975. *The Physics of Rubber Elasticity*, third ed. Clarendon Press, Oxford.
- Treloar, L., Riding, G., 1979. A non-Gaussian theory for rubber in biaxial strain. I. Mechanical properties. *Proc. R. Soc. London, Ser. A* 369, 261–280.
- Wall, F., 1943. Statistical thermodynamics of rubber. II. *J. Chem. Phys.* 10, 485–488.
- Wang, M., Guth, E., 1952. Statistical theory of networks of non-Gaussian flexible chains. *J. Chem. Phys.* 20, 1144–1157.
- Wu, P., van der Giessen, E., 1993. On improved network models for rubber elasticity and their applications to orientation hardening in glassy polymers. *J. Mech. Phys. Solids* 41, 427–456.
- Yamamoto, M., 1956. The visco-elastic properties of network structure I. General formalism. *J. Phys. Soc. Jpn.* 11, 413–421.
- Yamamoto, M., 1957. The visco-elastic properties of network structure II. Structural viscosity. *J. Phys. Soc. Jpn.* 12, 1148–1158.
- Yeoh, O., 1993. Some forms of the strain energy function for rubber. *Rubber Chem. Technol.* 66, 754–771.